REPUBLIC OF TÜRKİYE
AYDIN ADNAN MENDERES UNIVERSITY
GRADUATE SCHOOL OF NATURAL AND APPLIED SCIENCES
MASTER'S PROGRAMME IN MECHANICAL ENGINEERING
2023-YL-057

INVESTIGATION OF THE LOW-COST PASSIVE ON-CHIP CELL SEPARATION METHODS

Osman GÜLER

MASTER'S THESIS

SUPERVISOR

Asst. Prof. Dr. Sinan GÜÇLÜER

AYDIN–2023

ACCEPTANCE AND APPROVAL

The thesis titled "Investigation of the Low-Cost Passive On-Chip Cell Separation Methods", prepared by Osman GÜLER, a student of Department of Mechanical Engineering at T.C. Aydın Adnan Menderes University, Graduate School of Natural and Applied Sciences, was accepted as a Master's Thesis by the jury below.

Date of Thesis Defence: 18/07/2023

Member (T.D.)	: Asst. Prof. Dr. Sinan GÜÇLÜER	Aydın Adnan Menderes Üniversitesi	……
Member	: Asst. Prof. Dr. Adem ÖZÇELİK	Aydın Adnan Menderes Üniversitesi	……
Member	: Asst. Prof. Dr. Fikret SÖNMEZ	Manisa Celal Bayar Üniversitesi	……

APPROVAL:

This thesis was approved by the jury above in accordance with the relevant articles of the Aydın Adnan Menderes University Graduate Education and Examination Regulations and was approved on the ..... by from the Board of Directors of the Graduate School of Science in the ..... numbered decision.

Prof. Dr.Mustafa SÜRMEN

Institute Director

ACKNOWLEDGEMENTS

First of all, I would like to express my sincere thanks to my advisor Asst. Prof. Dr. Sinan GÜÇLÜER for his sincere, patient and dedicated support from the beginning of the process. Likewise, I would like to thank Asst. Prof. Dr. Adem ÖZÇELİK for the perspective and information he provided me throughout the process.

I would like to thank my dear friend and supporter Usama Rehman, who has been with me throughout this journey and never withheld his support.

I would also like to express my gratitude to my dear sister Hasibe Nur GÜLER, who believed in me and helped me throughout my master's program.

Finally, I would like to express my gratitude to my beloved mother Funda GÜLER and my beloved father İlyas GÜLER, who raised me with love and added a lot to me with their outlook on life and determination.

Osman GÜLER

TABLE OF CONTENTS

LIST OF SYMBOLS AND ABBREVIATIONS

µl **:** Microliter

µm **:** Micrometer

2D **:** Two-Dimensional

3D **:** Three-Dimensional

POC **:** Point-Of-Care Diagnostic Tool

TAS **:** Total Analysis Systems

FACS **:** The Fluorescence-Activated Cell Sorting

IVD **:** Intervertebral Disk

PZT **:** Piezoelectric Transducer

DEP **:** Dielectrophoresis

MACS **:** Magnetic-Activated Cell Sorting

SSAW **:** Standing Surface Acoustic Waves

IDT **:** Interdigital Transducers

PFF **:** Pinched Flow Fractionation

SNP **:** Single Nucleotide Polymorphisms

PCR **:** Polymerase Chain Reaction

DLD **:** Deterministic Lateral Displacement

CTC **:** Circulating Tumor Cell

PMMA **:** Polymethyl Methacrylate

CMOS **:** Complementary Metal-Oxide-Semiconductor

FEA **:** Finite Element Analysis

FEM **:** Finite Element Modeling

LIST OF FIGURES

LIST OF TABLES

ÖZET

DÜŞÜK MALİYETLİ ÇİP ÜSTÜ PASİF HÜCRE AYRIŞTIRMA METOTLARININ ARAŞTIRILMASI

Osman G. Aydın Adnan Menderes Üniversitesi, Fen Bilimleri Enstitüsü, Makine Mühendisliği Programı, Yüksek Lisans Tezi, Aydın, 2023.

Amaç: Bu çalışmada, literatürde en yaygın kullanılan pasif ayırma tekniklerinden biri olan Ataletsel Odaklama yöntemini kullanarak mikroakışkanların ayrılması hedeflenmeştir. Parçacıkların cihaz duvarlarıyla ve birbirleriyle etkileşimi büyük ölçüde cihaz yapısına bağlıdır. Sonuç olarak lazer kesim ve sayısal simülasyonlarda kullanılmak üzere elde edilen iki ayrı mikroakışkan cihazı analiz ederek sonuçların birbiri ile tutarlılığı hakkında bilgi sahibi olunması amaçlanmıştır.

Materyal ve Yöntem: Bu tez çalışmasında farklı yoğunluktaki hücrelerin ayrılması sırasında oluşan akışkan parametreleri incelenmiştir. Deneysel kısımda kullanılan cihaz CO_2 lazer kesim ile elde edilmiştir. Sıvı enjeksiyonu ve canlı, ölü hücre oranlarının karakterizasyonu sırasında ise bir şırınga pompası ve manuel hemasitometre kullanılmıştır. Sayısal analiz kısmında ise kullanılan programdaki modüller ve sonlu elemanlar yöntemi hakkında bilgiler verilmiştir.

Bulgular: Deneysel çalışmada, 1 ila 5 mikrometre arasında değişen polistiren partiküller mikroakışkan cihaza farklı akış hızlarında enjekte edilerek hareketli görüntüler elde edilmiştir. Serpantin bölümünde odaklanmış bir akış gözlemlenmiştir. Cihazın ayırma verimliliği 600 µl/dak ile 1000 µl/dak arasındaki akış hızlarında en yüksek seviyeye ulaşmıştır. 800 µl/dak giriş akış hızında en yüksek saflık (%93 ve %89) elde edilmiştir. Nümerik simülasyonda ise 2 partikülün yoğunluğu 1100 kg/m^3 olarak alınmış ve giriş hızları 0,45 m/s olarak ayarlanmış, partikül ayırma uygulamalarında yaygın olarak karşılaşılan bir dizi partikül boyutunu temsil etmek üzere 1 µm ve 5 µm çapında partiküller seçilmiştir. Ayırma işlemi, hız profilleri ve partikül izleme modülleri ile izlenmiş ve başarılı ayırma teyit edilmiştir.

Sonuç: Araştırma, laboratuvar deneylerinde ve sayısal simülasyonlarda parçacık manipülasyonu ve ayırma için iki farklı spiral şeklin başarılı bir şekilde kullanıldığını göstermektedir. Bu bulgular, bu spiral şekillerin biyoloji, biyoteknoloji ve tıbbi teşhis alanlarında potansiyel uygulamalar sunarak seçici ayırmayı etkili bir şekilde gerçekleştirebileceğini göstermektedir. Çalışma, mikroakışkan tabanlı partikül ayırma yaklaşımlarının geliştirilmesine katkıda bulunmakta ve mikroakışkan cihazların tasarımı ve optimizasyonu için değerli bilgiler sağlamaktadır.

Anahtar Kelimeler: Çip-Üstü-Laboratuvar, CO_2 Lazer, Mikroakışkanlar, Nümerik Analiz, Pasif Parçacık Ayırma Teknikleri.

ABSTRACT

INVESTIGATION OF THE LOW-COST PASSIVE ON-CHIP CELL SEPARATION METHODS

Osman G. Adnan Menderes University, Graduate School of Natural and Applied Science, Department of Mechanical Engineering, Master's Thesis, Aydin, 2023.

Objective: This study aims to separate microfluidics using Inertial Focusing, one of the most widely used passive separation techniques in the literature. The interaction of the particles with the device walls and with each other is highly dependent on the device structure. As a result, it is aimed to analyze two separate microfluidic devices obtained for use in laser cutting and numerical simulations and to have information about the consistency of the results with each other.

Materials and Methods: In this thesis, the fluid parameters during the separation of cells of different densities are investigated. The device used in the experimental part was obtained by CO_2 laser cutting. A syringe pump and a manual hemacytometer were used for fluid injection and characterization of live and dead cell ratios. In the numerical analysis part, information about the modules in the program used and the finite element method are given.

Results: In the experimental study, polystyrene particles ranging from 1 to 5 micrometers were injected into the microfluidic device at different flow rates and moving images were obtained. A focused flow was observed in the serpentine section. The separation efficiency of the device was highest at flow rates between 600 µl/min and 1000 µl/min. At 800 µl/min inlet flow rate, the highest purity (93% and 89%) was achieved. In the numerical simulation, the density of the 2 particles was taken as 1100 kg/m3 and the inlet velocities were set to 0.45 m/s. Particles with diameters of 1 µm and 5 µm were selected to represent a range of particle sizes commonly encountered in particle separation applications. The separation process was monitored with velocity profiles and particle tracking modules and successful separation was confirmed.

Conclusion: The research demonstrates the successful use of two different spiral shapes in laboratory experiments and numerical simulations for particle manipulation and separation. These findings suggest that these spiral shapes can effectively achieve selective separation, offering potential applications in biology, biotechnology, and medical diagnostics. The study contributes to the development of microfluidic-based particle separation approaches and provides valuable insights for the design and optimization of microfluidic devices.

Key Words: Microfluidics, Lab-on-a-Chip, Passive Particle Separation Techniques, CO_2 Laser, Numerical Analysis.

1. INTRODUCTION

Microfluidic technology is concerned with the movement of minute quantities of fluids (such as microliters or nanoliters) through devices, systems, and geometries with dimensions on the micron or sub-micron scale. The number of publications that deal with this subject is growing by the day, and the reason why the topic is so popular in the scientific community is because it has many benefits, including the usage of a very small quantity (e.g., a microliter) of sample or reagent, a reduction in the risk of contamination, a low cost (e.g., for analysis or diagnosis), automation, and increased sensitivity, accuracy, and reliability (Murshed, 2021).

Microfluidic technology is an illustration of an interdisciplinary area that has found use in a variety of industries, including biomedicine, diagnostics, chemical analysis, the automobile sector, and electronics. The influence and significance of microfluidic technology may be seen in the many real-world applications it has, which include virus detection and bioanalysis, cell manipulation and separation. The two types of separation procedures are passive methods and active approaches. Passive methods attempt to separate the particles by modifying their hydrodynamic behavior using geometrically changed microchannels. Active methods, on the other hand, use physical force to achieve the same goal. Pinched flow fractionation, inertial focusing, deterministic lateral displacement and hydrodynamic sorting are examples of techniques that fall into the category of passive methods. Inertial focusing is a microfluidic-based passive cell separation approach that has been shown to be one of the most promising in recent years (Volpe et al., 2019; Zhao et al., 2020; Javi et al., 2022). As the cells move through the microchannels, they are subjected to the impact of fluid forces, which results in the separation of the cells based on their size and form. This method is especially helpful for applications such as cell-based assays and clinical diagnostics, which require exceptionally high levels of purity and efficiency. Inertial cell separation methods are a series of microfluidic techniques that use the physical qualities of cells, such as their size, shape, and deformability, to sort and separate them from other cells or pollutants. These properties include the cell's ability to change shape as well as its size and shape. Both serpentine channels and spiral microfluidics are examples of popular forms of inertial cell separation technologies (Guan et al., 2013; Jiménez et al., 2021; Ning et al., 2021; Amani et al., 2022).

Traditional techniques of cell separation can be improved in various ways, including throughput, sample volume, and purity, by utilizing either serpentine channels or spiral microfluidics. Both of these approaches offer similar benefits. These technologies also require relatively little external equipment and may readily be linked with other microfluidic devices. As a result, they are appropriate for a wide variety of applications, including cancer research, drug development, and point-of-care diagnostics. Even though passive microfluidic technologies are less complicated than active ones, the bulk of passive devices still require high-priced and difficult-to-obtain cleanroom microfabrication facilities, which are difficult to come by in developing nations (Unger et al., 2000; Qin et al., 2010). Even if there have been a few preliminary publications on 3D-printed microfluidic devices for cell separation, it is essential to have additional examples and demonstrations in order to develop and improve this field with tools that are both easier and more effective (Yin et al., 2020; Ozcelik, 2022). Therefore, additional research into low-cost fabrication alternatives to standard microfluidic devices is still required in order to realize the goal of developing cell separation applications that are affordable and easily accessible.

In this study, we present a microfluidic device that is simple and reasonably priced. Rapid laser prototyping with polymethyl methacrylate (PMMA) was used to construct it. To accomplish sheath-less cell separation, the apparatus is built with a single intake, a segment that is serpentine in shape, and a microfluidic channel that is spiral in configuration. Yeast cells and polystyrene particles with a diameter of 1 μm may be effectively separated using this microfluidic device in a proof-of-concept application. The effectiveness of the separation is 85%. The performance of the device seems promising for many different lab-on-chip applications, despite the fact that it is both straightforward and inexpensive.

In addition to the laboratory setup and experimental work, a comprehensive computational analysis was conducted using COMSOL to further enhance our understanding of the microfluidic separation process. A COMSOL simulation was performed to investigate the performance of a spiral geometry, which consists of a 2-revolution design. The simulation aimed to provide valuable insights into the velocity fields within the microfluidic device and the resulting particle separation phenomena.

The 'Laminar Flow' module and the 'Particle Tracing for Fluid Flow' module from COMSOL were used to do this. The 'Laminar Flow' module allowed us to calculate and visualize the velocity fields, providing a detailed understanding of the fluid behavior within

the microfluidic device. By simulating laminar flow, we were able to observe how the fluid flows through the channels, the velocity distribution, and the presence of any recirculation zones.

To analyze the paths of the particles and the effectiveness of particle separation, we traced them within the simulated fluid flow using the "Particle Tracing for Fluid Flow" module. This module incorporated the effects of lift forces, drag forces, and centripetal forces acting on the particles. By considering these forces, we gained insights into the complex interplay between fluid dynamics and particle behavior, which ultimately influenced the separation efficiency within the microfluidic device.

In order to represent the inlets and outlets of the microfluidic device, the simulation model had two inputs and two outputs. The inlet velocities were set at a consistent value of 0.45 m/s, representing the flow rate of the fluid entering the device. Two particles were injected simultaneously into the system, each characterized by different diameters. These particles had similar densities of 1100 kg/m^3, allowing us to study the influence of particle size on the separation process.

By conducting this comprehensive COMSOL simulation, we aimed to obtain valuable data regarding the velocity fields, particle separation, and the underlying forces at play. The simulation results provide deeper insights into the functionality and performance of the two-spiral geometry in achieving efficient particle separation. These findings contribute to the development and optimization of microfluidic devices for various applications, ranging from biomedical diagnostics to environmental monitoring.

2. LITERATURE REVIEW

Active methods and passive methods are the two basic categories for particle separation techniques

2.1. Active Separation Techniques

Active separation approaches involve the use of an external field (such as electric, optical, magnetic, or acoustic fields, among others) in order to separate the cells. The microscale barriers or the fluid flow alone are used to accomplish the cell separation. In this article, we will talk about some of the more typical active separation techniques.

2.1.1. The Fluorescence-Activated Cell Sorting

A specific population of cells is isolated using the fluorescence-activated cell sorting (FACS) technology from a heterogeneous mixture (including clinical and environmental materials) by examining the fluorescence and light scattering characteristics of each individual cell. Cell labeling can be done in a variety of ways; however, fluorescent nanoparticles, fluorescent proteins, and antibodies that have been labeled with fluorescent molecules are the most common types of reagents utilized in FACS analysis (Sivaramakrishnan et al., 2020). Because of its sensitive nature, extensive engineering development, and high throughput, FACS has become the method of choice for many scientists when it comes to the sorting of cells. It was first developed by Bonner, Hulett, Sweet, and Herzenberg (Bonner et al., 1972; Herzenberg and Sweet, 1976; Hulett et al., 1969). In the 1970s, Becton Dickinson Immunocytometry Systems was the company that first brought this method of cell sorting to the market for commercial use (Pandey, Mehendale and Paul, 2018).

The sample is first surrounded by a sheath fluid in the FACS (Figure 2.1) procedure, and then a nozzle focuses the fluid into a narrow stream. The flow of the material is altered in such a way that the distance between the cells is significantly greater than the size of each cell, allowing for the simultaneous detection of only a single cell.

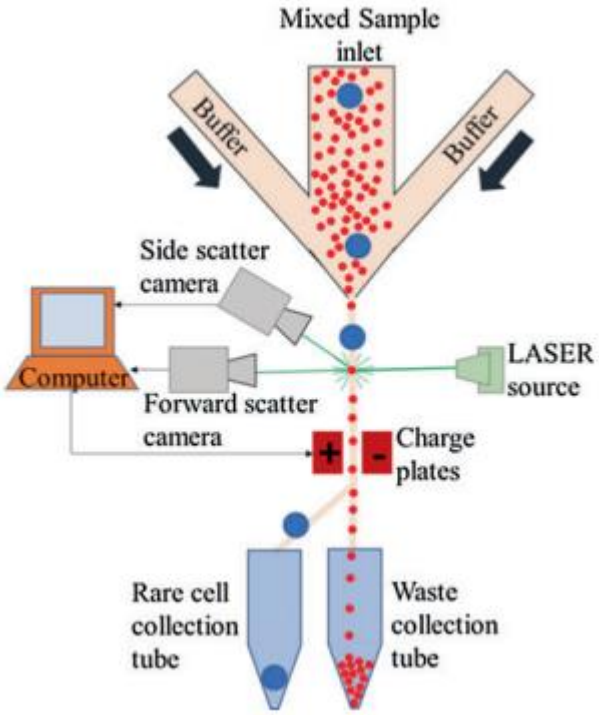

Figure 2.1. Using a technique called fluorescence-activated cell sorting (FACS), cells are first focussed so that only one cell can be seen by the laser at once. The discovered cells are then placed in a drop, given an electric charge, and divided into various categories by the deflector plates. (Pandey, Mehendale and Paul, 2018)

A laser is used to excite the fluorescently labeled antibodies in the detection zone. The fluorescence and scatter signals emitted by each cell as a result of this excitation are then detected by several detectors. Following the passage of a cell via the detecting zone, the stream is fragmented into droplets, and within each droplet is a single cell. On the basis of the fluorescence signal emitted by the cell that is contained within the droplet, an electric charge is applied to it. This charge can either be positive or negative. The charged droplet is guided to a tube via electrostatic deflection so that it can undergo additional examination (Pandey, Mehendale and Paul, 2018).

Cho et al. (2010) improved the microfluidic FACS device by including Teflon waveguides (optical detecting sources) positioned along the microchannel, an upgraded control system, and a PZT actuator to achieve automated high-throughput cell sorting. The microfluidic device that was created as a result is able to circumvent the most typical disadvantages, such as hydrodynamic shear stress-driven cell death and clogging and reach a high throughput of 2,174 cells per second (Sivaramakrishnan et al., 2020).

2.1.2. Dielectrophoresis

Dielectrophoresis (DEP) is a phenomenon that happens when a polarized particle is suspended in a buffer solution and an externally applied nonuniform electric field interacts with the induced unevenly distributed dipoles that are present in the polarized particle (Lewpiriyawong et al., 2011).

These kinds of interactions can result in a nonzero coulombic net force being exerted on the particle, which in turn causes the particle to move (Tay et al., 2007). In order to separate and sort particles and cells, microfluidic devices make full use of this physical phenomenon. The charge of the particles is not taken into account in this method. The dielectric characteristics of the particles and the surrounding electric field have a significant impact on the mobility of the cells or particles. Therefore, in the presence of electric fields, each cell exhibits a distinct pattern of dielectrophoretic activity, which enables the cells to efficiently separate from one another and sort themselves (Sivaramakrishnan et al., 2020).

A dielectric typically consists of a polar substance with two randomly selected poles. According to the dipole moments of the polar molecules, when an external electric field is applied, both the particles and the fluid medium being used are polarized in one direction. As a direct consequence of this, surface charges begin to build up at the point where the particles and the fluid meet. In order to redirect the electric field that was initially present, a supplementary electric field is produced (Figure 2.2.) (Coşkuner, 2014).

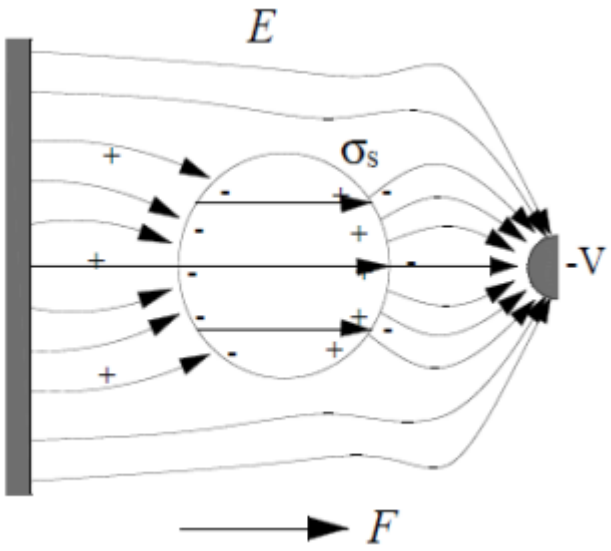

Figure 2.2. Interfacial Polarization And Dielectrophoresis

Because of the unequal distribution of the electric field, the interactions between surface charges and the electric field ultimately result in a net force being exerted on the particle. The vast majority of studies, on the other hand, make the assumption that surface charges are sufficiently negligible to behave as bipolar charges in the same direction as the electric field. The relationship given below defines the DEP force:

$$\vec{F} = \int_0^V (\vec{P} \times \nabla)\vec{E}dv \qquad (1)$$

In this equation, P denotes the dipole moment, and E is the strength of the electric field that is present externally. The DEP force operating on a microscopic spherical particle can be calculated using the equation:

$$\vec{F} = 2\pi a^3 \times \varepsilon_m K \nabla E_0^2 \qquad (2)$$

The radius of the spherical particle is given by an in the equation, and F stands for the DEP force that is being applied in the direction of the electric field. In this equation, the Clausius-Mossotti factor, symbolized by the letter K, is established as follows:

$$K = \frac{\varepsilon_P - \varepsilon_m}{\varepsilon_p + 2\varepsilon_m} \qquad (3)$$

ε_P and ε_m symbolize the permeability of the particle and the fluid. The sign of K is what decides which way particles will move relative to one another. If K is greater than zero,

the particle goes in the direction of regions with a high electric field; if K is less than zero, the particle moves in the opposite direction. In order to fine-tune the effective separation, it is required to alter the DEP force, which is generated when an electric field of varying frequencies, magnitudes, and directions is applied (Coşkuner, 2014).

DEP microfluidic systems have advanced significantly since the work of Pohl, who initially demonstrated the separation of polystyrene particles using wire electrodes of diameter 0.258 μm-1.59 μm that were put in between glass slides (Pohl et al., 1978). Pohl utilized wire electrodes in his experiment to separate the polystyrene particles. These microfluidic devices were not only bulky, but also lacked the cell specificity required to isolate a certain cell or particle type.

Over the course of the last few decades, microfabrication techniques (photolithography and soft lithography) have been used to miniaturize DEP microfluidic devices. These techniques allow for even electrodes with a diameter of 100 μm to be included in order to increase the performance of DEP devices (Minerick et al., 2003). In addition to decreasing the size of the electrodes, researchers have also experimented with a wide variety of electrode shapes and geometries (Sivaramakrishnan et al., 2020).

2.1.3. Magnetic-Activated Cell Sorting

The term "MACS" refers to magnetic-activated cell sorting, which was developed by Miltenyi et al. (1990) to address the throughput issues with FACS. The first step of magnetic cell sorting is the incubation of sample cells in magnetic beads containing the recognition molecule (antibodies), as opposed to fluorescence. "Magnetic labeling" is the term used to describe this (Bhagat et al., 2010).

In Figure 2.3., antibody-coated magnetic beads with a diameter of less than 100 nanometers specifically bind to a certain protein that is located on the surface of the cell that is to be examined. The cells that have been magnetically tagged are moved through a column of steel wool that has been positioned in a magnetic field gradient created by permanent magnets. In the presence of the magnetic field, the tagged cells are collected by the column, while the unlabeled cells are removed by the washing process. In order to elute cells that are attached to the column, the magnetic field must first be turned off. During the process of

enrichment, which is also referred to as "positive separation, the cells that are sought are marked with coated magnetic beads, and the cells that are not marked are thrown away. In the instance of depletion, which is sometimes referred to as negative separation, the unneeded cells are marked with a marker and then trapped by the magnetic field (Pandey et al., 2018).

Because of the magnetic force that is provided, these types of microfluidic systems have flow patterns that are generally parallel to one another and do not have any obstructions in the primary direction that fluid is flowing. As a result, this technique is suitable for analyzing magnetically induced biological particles without distorting the particles' original forms (Pamme, 2007).

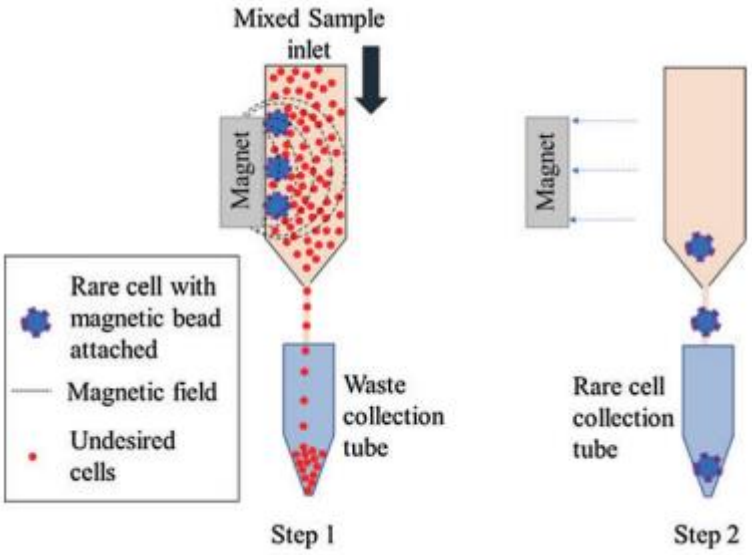

Figure 2.3. Magnetic nanometer-sized beads coated with antibodies are attached to the cells of interest to perform magnetically activated cell sorting (Pandey et al., 2018).

2.1.4. Optical Method

Ashkin was the first person to invent the concept of optical manipulation by utilizing an optical tweezer to capture and transport individual cells, particles, or molecules by generating an optical force on the particle based on the particle's size, shape, and refractive index (Ashkin & Dziedzic, 1987). Optical manipulation was initially developed by Ashkin. Because the application of an optical force perpendicular to the flow is able to deflect the particle paths in a microchannel, the optical force is currently being widely implemented for

particle separation in microfluidics. This has been the case for some time. Optical manipulation has also found uses in the field of biophysics, where it has been used to examine the mechanical properties of cells, such as stiffness and deformability. Optical manipulation has also found applications in the field of engineering. Additionally, because optical tweezers are able to apply exact forces to minute objects, they have become a valuable tool for micromanipulation in a variety of domains, such as materials science and nanotechnology. (Bhagat et al., 2010).

The optical polarizability of a particle or cell is what determines whether or not it will be affected by an optical force. Sorting can be accomplished on the basis of differences in the particle size or the refractive index of the material. The refractive index was used by MacDonald and colleagues to demonstrate the separation of two distinct types of particles (MacDonald et al., 2003).

They put a buffer solution and a suspension with a mixture of silica particles with a size of 2 μm and polymer particles with a size of 2 μm into an H-shaped channel device. The n value of the silica particles was 1.73, and the n value of the polymer particles was 1.58, respectively. The polymer particles, on the other hand, were diverted into the buffer-carrying stream as they moved through the optical field, while the silica particles continued to flow unimpeded. At a flow rate of 30 μm/s, sorting was carried out with an efficiency of over 100 percent, which corresponds to a throughput of around 25 particles s-1. At a flow rate of 20 μm/s, the same apparatus was also put to use to deflect protein capsules with a diameter of 2 μm and separate them from a mixture of capsules with a diameter of 4 μm. More recently, the same group revealed how to separate a mixture of silica particles with varying sizes, including 2.3 μm, 3.0 μm, 5.3 μm, and 6.8 μm (Milne et al., 2007). One other example of a process that does not involve intrusive procedures is optical sorting. Because separation is accomplished through the use of inherent qualities, labeling is not necessary. There is a degree of independence between the optical force and the flow rate that can be modified. This technique can be utilized for the analysis of inorganic, polymeric, and biological particles. In addition, it has been demonstrated that optical sorting is a versatile method for separating particles according to their shape. This is due to the fact that the optical force can be highly sensitive to the geometry of the particle. In addition, recent advancements have made it possible to use several optical traps for the simultaneous sorting and manipulation of various types of

particles. This has opened up new opportunities for high-throughput and sophisticated microfluidic applications (Pamme, 2007).

2.1.5. Acoustic Method

A radiation force that can be utilized to control particles and molecules can be created when a piezoelectric material is used to induce ultrasonic acoustic resonance (standing waves) inside of a microchannel. The separation of blood cells, including platelets, red blood cells, and leukocytes, as well as beads with sizes ranging from 2 μm to 10 μm, was demonstrated by Petersson et al. (2007) using free flow acoustophoresis (Figure 2.4). The force and temperature increases that the cells experience while they are in the acoustic standing wave were examined by Evander et al. in 2007. The survival of the cells within the radiation force field could be a problem for this procedure, hence this was done. More than 15 minutes passed during which the neural stem cells contained in the trap remained alive.

The maximum force that the cells encounter is on the order of 0.5 nN, which is comparable to the forces produced by other manipulative techniques like optical trapping. In reality, the control, concentration, and trapping of cells have all benefited by the application of acoustic standing waves. Johansson et al. (2009) used acoustic cell manipulation to alter the flow of cells in a microfluidic FACS device. Norris et al. (2009) used an acoustic standing wave inside the microfluidic channel to extract sperm cells from epithelial cell lysate for the aim of performing forensic DNA analysis. To ensure that the acoustic power is effectively communicated to the fluid, the materials used to construct the device must be carefully chosen due to the nature of the system (Laurell et al., 2007).

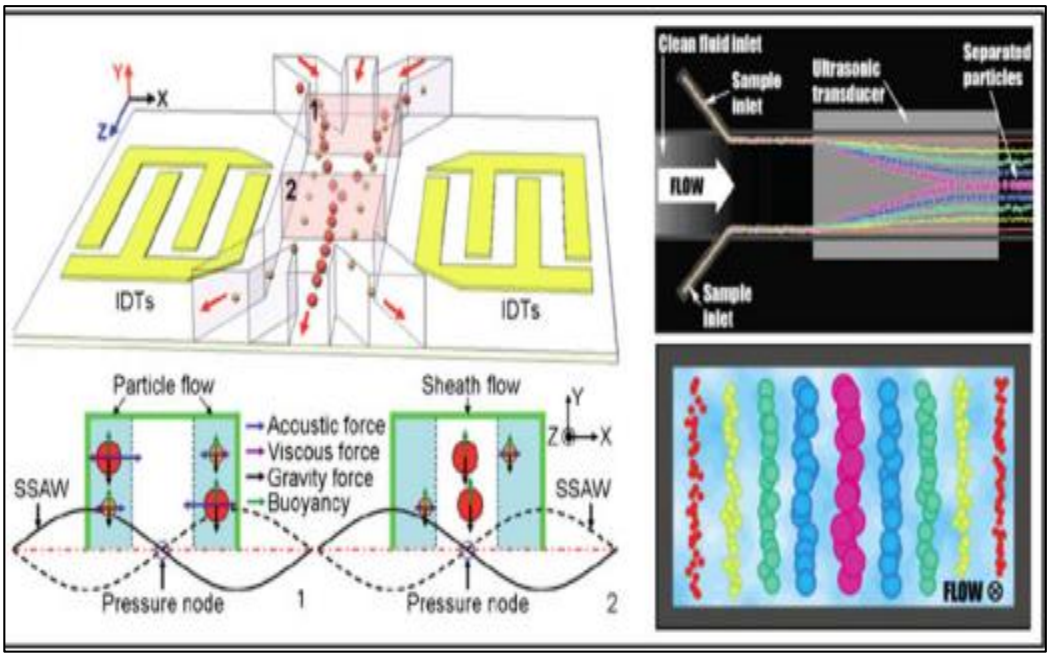

Figure 2.4. Acoustic separation. right Schematic illustrating the principle of acoustic separation by standing surface acoustic waves (SSAW) generated using interdigital transducers (IDT). The varying acoustic forces repositions the larger cells closer to the channel center and smaller cells farther from the center. (Shi et al., 2009), copyright 2009, The Royal Society of Chemistry. left Illustration of a size-based acoustic fractionator using an ultrasonic transducer placed under the microchannel. Cells of varying sizes align at distinct positions across the microchannel crosssection based on the acoustic primary radiation force experienced. (Petersson et al., 2007), copyright 2007, American Chemical Society

2.2. Passive Separation Techniques

Active techniques may have a high separation performance, but they are still limited since they need to be integrated with other apparatus in order to supply an external field or specialized chemicals such as antibodies. This makes it difficult for active techniques to be used in isolation. On the other hand, passive approaches do not require the use of any external field as the driving force for separation and make use of label-free methods to separate nanoparticles. Instead, hydrodynamics and the forces acting at the surface are the key factors in the separation process.

Passive approaches have various advantages over active techniques. For instance, passive procedures do not necessitate the employment of any additional tools or substances; as a result, they are not only less expensive but also simpler to implement. In addition, passive approaches can be employed in a wider variety of situations, such as those with limited resources or at the point of care, where access to specialist equipment or reagents may be limited.

In addition, passive approaches can be less harsh on the particles, lowering the likelihood that their properties would be altered or damaged as a result of the separation process. When working with delicate or fragile particles, such as biological cells or nanoparticles with sensitive surface coatings, this is of the utmost importance (Salafi et al., 2017).

2.2.1. Pinched Flow Fractionation

Yamada et al. (2004) originally introduced the innovative hydrodynamic chromatographic method known as PFF, or pinched flow fractionation, for conducting size-based separations in microchannels. A 'pinched segment' that is a component of the microchannel can be used to align particles to one of the sidewalls. Changing the flow rates of both fluids results in the creation of this segment. Particles tend to migrate in the direction of the streamline that passes through their centers of mass when the flow is laminar. The channel sides are closer to streams that travel via the centers of mass of smaller particles, while the centre of the channel is closer to streams that pass through the centers of mass of larger particles. The fluid and solid particles that are mixed together and are expelled by the pinched segment are sorted into their respective size categories by the spreading streamlines (Sajeesh & Sen, 2014).

Yamada et al. (2004) conducted research on the performance of separation using polystyrene particles with sizes ranging from 12 to 30 micrometers in diameter. In addition, the researchers investigated how the flow rate and channel designs impacted the results. They discovered that utilizing the PFF method, particles of varying sizes could be constantly and accurately separated from one another, and that the particle size could be calculated based on the effluent position. In addition to this, they discovered that the geometry of the

microchannels had an effect on the performance of the separation, which is in line with the notion that the behavior of particles is mostly dictated by the particular flow profile.

(Yamada & Seki, 2005) reported an original strategy that made use of PFF in a separate investigation that they conducted. They discovered that high separation performance could be achieved by building a drain channel to receive a considerable amount of the liquid flow. This allowed for the liquid flow near one side wall to be properly spread, which allowed for high separation performance. In a microchannel with a pinched segment width of 20 μm, a combination of particles ranging in size from 1.0 to 5.0 μm was successfully separated. In addition, they improved the separation yield by incorporating check valves into the design of the channel. This, in conjunction with the utilization of PFF, allowed them to achieve quite high separation yields, which were close to 90% (Yamada, 2006).

PFF was recently utilized in the research conducted by Larsen, Poulsen, Birgens, Dufva, and Kristensen (2008) to locate point mutations in the HBB gene using functionalized polystyrene microspheres with diameters of 3.09 μm and 5.6 μm, respectively. By incorporating biotin-labeled oligonucleotides into the microspheres, it was possible to distinguish between a wild-type (Wt) and mutant (Mt) DNA sequence in the HBB gene. By using fluorescent targets made of artificial DNA oligonucleotides or amplified RNA that had been made from human DNA samples acquired from people who had point mutations in the HBB gene, it was possible to achieve hybridization to functionalized beads. The beads were thoroughly washed, then separated using a PFF apparatus and the fluorescent signal coming from the beads was analyzed. Patients that were either wildtypes, heterozygotes, or mutants for the examined mutation were able to be correctly diagnosed using the PFF device. This demonstrates that the PFF method is applicable to accurate and rapid genotyping of SNPs (Bhagat et al., 2010).

In addition, the PFF method has the possibility of being used for purposes other than the genotyping of single nucleotide polymorphisms (SNPs). It is possible, for instance, to employ it for the identification and analysis of various forms of genomic changes, such as insertions, deletions, and copy number variants. PFF can also be integrated with other molecular techniques to enable the multiplexed investigation of a number of genetic targets at the same time. This has the potential to significantly boost the efficiency and throughput of genetic testing, particularly in clinical settings where timely and correct diagnosis is of the

utmost importance. In order to fully exploit the potential of this strong technology, additional research and development of PFF-based assays are necessary.

PFF is superior to other microfluidic cell separation technologies in a number of ways and offers several advantages as a separation technique. Cells of varied sizes can be effectively separated using the same device by adjusting the ratio of the flow rates of the sample and the sheath buffer. This is possible due to the fact that the separation efficiency is only dependent on the laminar flow profile in the pinched and expanded segments. PFF can also be integrated with other techniques for conducting analyses further downstream, which enables the processing of separated cells to be carried out in a quick and effective manner. For instance, isolated cells can be studied with high-throughput sequencing, single-cell PCR, or mass spectrometry, which can provide useful information regarding cell populations and the roles they perform (Bhagat et al., 2010).

In addition, the process of particle separation in PFF has been investigated computationally using techniques like the boundary-integral approach and the lattice Boltzmann method (Shardt et al., 2012; Risbud and Drazer, 2014). These methods provide a roadmap for the development of PFF microdevices in the future. In addition, the utilization of computer simulations has the potential to facilitate the optimization of PFF separation efficiency as well as the reduction of the experimental time and associated expenses associated with device optimization. Additionally, computational approaches can help uncover potential issues and limitations in the PFF technique, which in turn makes it easier to build new solutions to address such challenges and constraints (Lu & Ye, 2015). As a result, PFF offers a significant amount of untapped potential across a broad spectrum of biological and medicinal applications.

2.2.2. Deterministic Lateral Displacement

A method for the creation of flow streamlines known as deterministic lateral displacement (DLD) makes use of a framework consisting of pillar arrays that are inclined at an angle. The DLD method of microparticle separation has seen widespread use for the separation of circulating tumor cells, blood cells, mammalian cells, spores, parasites, and bacteria, among other types of particles. The researchers Huang et al. found that in a laminar

flow, the number of streamlines that were formed in the gap that was caused by the row shift might result in size-based separation (Huang et al., 2004).

Recent developments in DLD technology have suggested that it may be possible to separate complicated mixtures while maintaining a high level of resolution and specificity. In addition, the DLD method can be integrated with other methodologies, such as fluorescence microscopy and microfluidic sorting, which enable additional examination and manipulation of the particles that have been separated. It is necessary to do additional research in order to investigate the full potential of microdevices based on DLD for use in a variety of applications in the biomedical and industrial fields.

Along the bumping mode, particles that were larger than the first streamline displaced laterally, and particles that were smaller than the first streamline flowed in a zig-zag pattern through the pillars without causing any lateral displacement, as demonstrated in Figure 2.5.. The cut-off diameter between these trajectories is denoted by the device's critical diameter (sometimes abbreviated as D_c). An empirical formula for determining the critical diameter was developed by Davies et al. based on their research into the effects of varying device gaps (G), shift fractions ε, and particle sizes.

$$D_c = 1.4 \times G \times \varepsilon^{0.48} \quad (4)$$

This DC formula calls for a device to have a small gap or row shift fraction if it is going to be used to separate nanosized particles. A low row shift fraction design, on the other hand, requires a wider separation region, which increases the diffusion length. A tiny gap size, on the other hand, adds to high channel resistance and fabrication complexity. Alternately, as the cut-off diameter of various pillar forms, such as triangle, I-shaped, or asymmetric gap, is less than that of normal circular DLD arrays, the separation of tiny particles may be improved by employing alternative pillar shapes, such as triangle, I-shaped, or asymmetric gap.

There was a previous review that was published on the topic of deterministic lateral displacement. DLD has been utilized in a number of different failed attempts to separate submicron particles. Polystyrene beads measuring 600 nm and 800 nm were separated using a device that was built by Huang and colleagues, the inventors of DLD. The device had a distance of 1.6 meters and a row shift fraction of 0.1. Using a DLD device with a critical diameter of 250 nm, Santana et al. (2014) was able to successfully separate fluorescence-labeled particles measuring 190 nm in size from beads measuring 2 m in size. In addition,

Zeming et al. (2016) developed a DLD pillar array with a spacing of 2 meters to differentiate between particles measuring 350 nm.

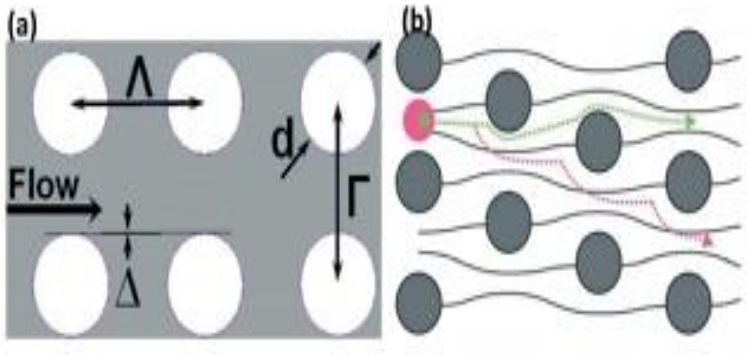

Figure 2.5. DLD Separation on Nanoparticles. (a) DLD Design Parameters, (d as pillar diameter, Γ and Λ as row and column periods, respectively, Δ is the shift fraction) (b) Nanoparticles Movement Differences Due to Their Size (Joensson et al., 2011; Santana et al., 2014)

Despite the fact that this method is straightforward and has seen extensive use for microparticles, the presence of a substantial number of pillars causes issues regarding relatively low throughput and channel clogging. This is the case even though the method in question is basic. Furthermore, the effect of diffusion is larger for nanosized particles, which decreases separation efficiency because it causes a broad dispersion of particles in the outlet channel. This is caused by a broad distribution of particles in the outlet channel.

2.2.3. Hydrodynamic Separation

The techniques of hydrodynamic separation are appropriate for laminar flows with a low Reynolds number and the behavior of cells in those flows. The hydrodynamic lift force that a cell experience is dependent on its size, shape, and deformability, and it is this force that causes the cell to adhere to a streamline as it travels through the channel (Jackson & Lu, 2013). Because of this, the amount of force that each cell is subjected to will vary according to the features that define it, and the cell will also occupy a variable position. When a

microchannel divides into various branches, particles will have a tendency to follow distinct streamlines depending on where they were initially situated. This is done in order to achieve a distinction based on size. This method can be carried out using microchannel bifurcation, pinched flow fractionation, or the so-called "biomimetic" behavior (Autebert et al., 2012).

Microchannel bifurcation is an efficient method for separating cells into distinct populations based on their dimensions. In this method, there is a channel that is divided into two branches; typically, the larger cells will enter one of the branches, while the smaller cells will enter the other branch. On the other hand, pinched flow fractionation utilizes a channel that is constricted to a much smaller width than the rest of the channel in order to sort particles according to their size. In biomimetic separation, cells are separated according to size by using customized microstructures that imitate the blood veins found in the human body (Shiri et al.). This technique was inspired by the movement of cells as they passed through blood vessels. In general, hydrodynamic separation techniques provide a promising strategy for the separation of cells and particles based on their size and physical properties. Furthermore, these approaches have the potential to be applied in a wide variety of sectors, including clinical diagnosis and biomedical research.

The Zweifache-Fung effect, commonly referred to as the bifurcation law, can be utilized through the use of the bifurcation method. This phenomenon was discovered for the first time by Yang et al. (2006), and it fundamentally suggests that in different bifurcations, the differences in flow velocities will lead to the separation of the cells. The movement of red blood cells was tracked in the research carried out by Yang et al. (2006), and it was used to make a comparison between the blood flow in blood veins and capillaries. These cells tend to move into the daughter vessel when they reach the bifurcating zone of a capillary blood channel because it has a higher flow rate, but very few cells do so (Fung, 1973). There are also works that are comparable to this found in (Jäggi et al., 2006; Zheng et al., 2008).

One other application of the bifurcation approach is shown in the form of the herringbone construction. The apparatus features branches that can split off in two different directions: to the left and to the right. The first proposal for this technology suggested using it to centralize particles. A helical flow and many vortices are produced as a result of the unintentional and irregular movement of the flow that is caused by the continual changes in direction. The particles end up being concentrated more effectively as a result of such

movement (Shah, 2018). Additionally, the herringbone shape is utilized in channels whose inner and outer surfaces are coated with antibodies to segregate CTCs. As can be seen in Figure 2.6. (Stott et al., 2010), many directional shifts within these structures lead to an increase in the amount of mixing that occurs between the cells and the antibodies. In addition, modeling and simulation of this structure have been carried out so that the geometry can be improved, and the yields can be increased.

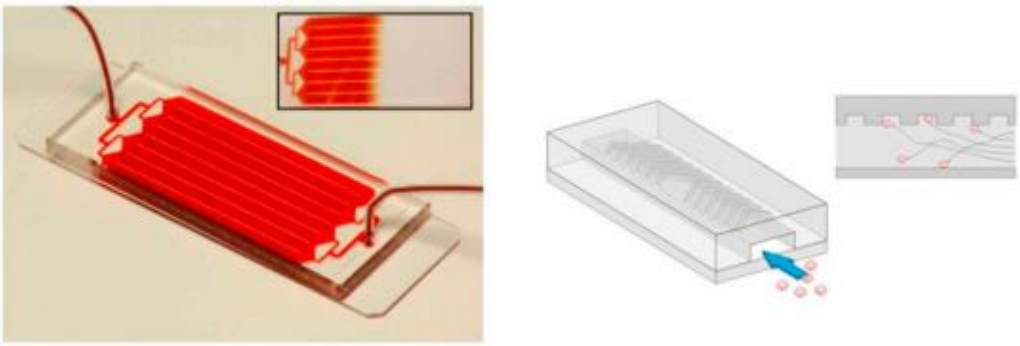

Figure 2.6. Herringbone Pattern-Based Device for Isolating CTC's (Stott et al., 2010)

2.2.4. Effect of Inertial Forces and Lateral Migration in Microchannels

There are two inertial lift forces acting on a particle as it travels through a straight microchannel (Park & Jung, 2009):

(i) a shear-gradient-induced lift force

(ii) a wall-effect-induced lift force

These two forces are produced as a result of the particle's collision with the wall. The channel's internal velocity profile has a parabolic form, which causes the shear-gradient-induced lift force. In compared to the side of the particle farther from the centerline, the wall side of a spherical particle at the channel centerline exhibits a higher gradient in velocity (Asmolov, 1999). Therefore, the spherical particles roll outward from the center in the direction of the walls of the microchannel.

The 'wall-effect-induced lift force' can be understood when the flow field surrounding a spherical particle is taken into account in the presence of a wall that disrupts the flow and results in the generation of an asymmetric wake around the particle. The particles are pushed

away from the wall by a lift force that is produced as a result of the wake's asymmetry. Because the two lift forces will be acting in opposite directions, particles in the microchannels will migrate laterally. This technique allows the sorting of particles of different sizes since the location of the particles within the microchannel cross-section depends on their size in respect to the microchannel's dimensions. The first to offer proof that lateral migration was a real event was Segre and Silberberg (1961). According to the findings of their experiment, particles move at a particular location, which is located approximately 0.6 of the tube's radii away from the tube's axis. It was observed that the tubes with circular and rectangular cross-sections produced results that were comparable (Kim & Yoo, 2008; Shao et al., 2008). Studies conducted much later have demonstrated that the behavior of lateral migration can also be influenced by characteristics such as the shape of the particle, its deformability, and the viscosity of the fluid that it is surrounded by. When compared to spherical particles of the same size, non-spherical particles, for instance, are subject to differing lift forces and may migrate in a manner that is distinct from the latter. Additionally, the viscosity of the fluid has an effect on the flow field that surrounds the particles and has the potential to change the behavior of migration (Bayareh & Mortazavi, 2009). For the purpose of optimizing the design and operation of microfluidic devices for particle separation, it is essential to have an understanding of these parameters.

As the particles go from one contraction to another through the expansion chamber (multi-orifice microchannel), as depicted in Figure 2.7. (Park & Jung, 2009), there is a transfer of momentum between the particle and the fluid. The decrease in momentum and the ensuing inertial force are both lessened since there isn't a large mismatch between the particle's route and the fluid's path during the initial transition between 1-2 and 2-3. There is a large change in the particle's momentum when it moves from area 3 to region 4, and the direction of the induced lift force is acting in a direction that is toward the wall as a result of the fluid and particle routes not matching. Regardless of the size of the particle, if there is a wall present, the particle will align itself in the direction of the wall. This alignment is caused by the presence of the wall. The transition of particles from position 4 to position 5 is an extremely important step. In this case, both the mismatch in the path and the ensuing change in momentum are important. In addition, the induced lift force is applied in a direction that is away from the wall.

The following describes this lift force:

$$F_L = \frac{\rho_p \pi d^3 U^2}{6D_h} \quad (5)$$

Where p represents the density of the particle, d represents its diameter, U represents the average flow velocity, and Dh represents the hydraulic diameter of the channel. The equilibrium position of the particle is obtained when the inertial force and the drag force are in equal and opposite balance with one another. The following expression can be used to determine the particle's velocity as it moves laterally:

$$U_d = \frac{\rho_p d^2 U^2}{18\mu D_h} \quad (6)$$

where the fluid's viscosity, in which the particle is travelling, is. It has been found that the lateral migration of particles is inversely proportional to the square of the particle diameter and the fluid flow rate. As a result, the larger particles are separated from the smaller particles by a larger lateral shift.

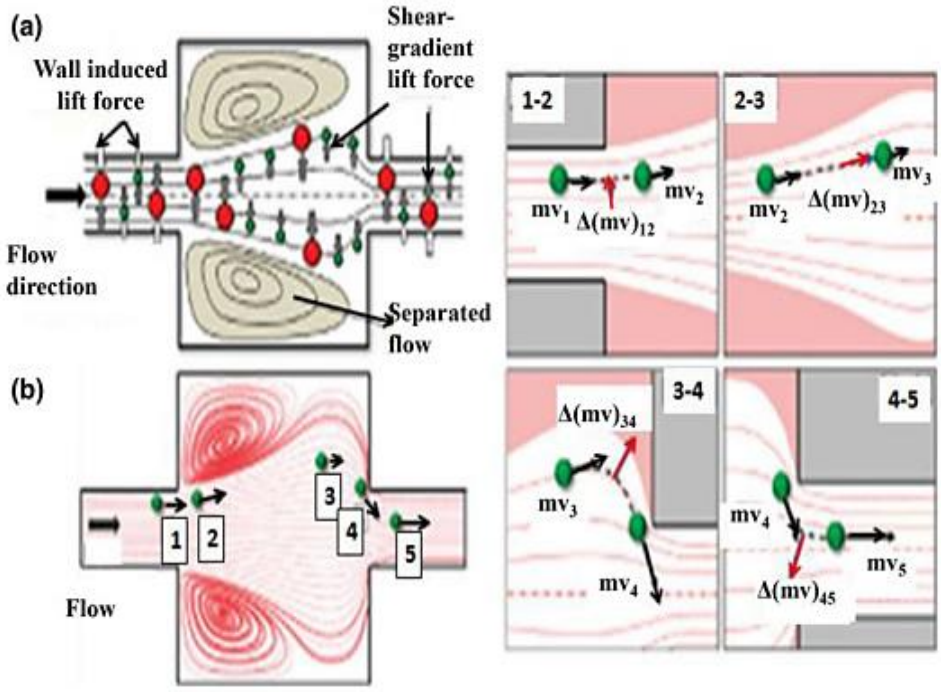

Figure 2.7. (a) The Flow in a Straight Channel Between Two Pairs of Contraction-Expansion. (b) The Path of Particles with Momentum Exchanges Between the Fluid and the Particle (Park & Jung, 2009)

The majority of biomedical suspensions consist of particles that are deformable (Hood et al., 2013). For instance, in comparison to healthy cells, cancer cells are significantly bigger and more malleable (Suresh, 2007). On deformable particles, as opposed to rigid particles, a deformability-induced lift force acts, which results in a difference in the dynamics of the two types of particles (Bayareh & Mortazavi, 2009; Mortazavi & Bayareh, 2009; Bayareh & Mortazavi, 2011; Schaaf & Stark, 2017). Schaaf and Stark (2017) conducted research on the mobility of an elastic capsule inside a microchannel. Their findings showed that the deformability of the capsule forces it in the direction of the centerline of the channel. They came to the conclusion that the final equilibrium location of a deformable capsule is influenced both by its size and its ability to deform. A further point to consider is that the bulk Reynolds number does not have a significant impact on the migration mechanism. It is crucial to stress that deformability can be controlled by varying the Webber number, the Eotvos number, the capillary number, the ratios of density and viscosity, as well as other parameters.

3. MATERIAL AND METHOD

3.1. Laboratory Setup

In this section, apart from the production and working principles of the device used during laboratory studies, information about the definition, properties and how to use the CO_2 laser cutter, syringe pump and hemocytometer equipment is given.

3.1.1. Hemocytometer

A specific glass slide that has been etched with a grid on its surface is known as a hemocytometer. Counting and determining the concentration of cells or particles in a liquid sample are both possible with its help when performing microscopy. Because the grid is made up of numerous squares, each of which has a specified dimension, accurate cell counting and volume estimation are now possible. One can determine the cell concentration in the primary sample by counting the cells within a predetermined area after placing a diluted sample on the hemocytometer and studying it under a microscope. This allows one to extrapolate the cell concentration that was present in the first sample. In the domains of hematology, microbiology, and cell culture, in particular, hemocytometers are a popular tool utilized in the research that is conducted in medical and biological fields.

In biological and medical laboratories, a commonly used method for counting the number of cells in a sample involves the utilization of a hemocytometer. To perform cell counting, the following step-by-step guide outlines the process of utilizing a hemocytometer:

Preparing the hemocytometer

Ensure thorough cleaning of the hemocytometer, removing any particles or residue from its surface. This is typically accomplished by cleaning it with 70% ethanol and wiping it down with a lint-free tissue or cloth. Confirm that the coverslip is securely positioned on top.

Preparing the cell suspension

Thoroughly mix the contents of the cell suspension to ensure an even distribution of cells. In cases where cells are clumped together, careful disaggregation can be achieved using a pipette or vortexing technique, taking care to avoid cell damage.

Loading the hemocytometer

Using a pipette, gently and gradually introduce a small volume of the cell suspension into the V-shaped groove located between the coverslip and the counting chamber. The volume introduced should range between 10 and 20 microliters. Capillary action will draw the cells into the chamber. It is important to avoid overcrowding the chamber, as it may lead to inaccurate cell counts.

Setting up the microscope

Place the hemocytometer, already containing the sample, onto the microscope stage and adjust its position so that the counting chamber is centered within the field of vision. To visualize the cells in their entirety, employ a 10x or 20x objective lens, depending on the cell size. Make necessary adjustments to the microscope focus.

Counting procedure

Initiate cell counting by starting from a known location within the middle grid's four large corner squares, systematically moving across the grid. Include cells that touch the top or left boundary of a square while excluding those touching the bottom or right boundary. Count only cells entirely contained within the square, disregarding cells on the perimeter lines.

Repeat the counting

To obtain an average count, multiple squares on the grid should be counted using the aforementioned method. This approach minimizes inaccuracies and provides a more representative overall cell count. Counting cells in several squares and calculating the average cell count per square is a commonly employed technique.

Calculating cell concentration

Once the average count per square is determined, the cell concentration in the original sample can be calculated. The formula for cell concentration (cells/mL) is as follows: (Average count per square) / (Dilution factor) * (10^4). The dilution factor represents the extent to which the

original cell sample was diluted when applied to the hemocytometer. For instance, if ten microliters of cell suspension were added to a dilution of trypan blue solution at a ratio of one to ten, the dilution factor would be ten.

Analyzing and reporting the results

Thoroughly analyze the cell count and concentration data according to the experimental requirements. Document the findings and include any relevant observations or additional information.

It is important to remember that achieving accurate cell counting with a hemocytometer relies on employing proper techniques, maintaining attention to detail, and practicing consistently.

3.1.2. CO_2 Laser Cutter

A carbon dioxide (CO_2) laser is the kind of laser that's used in a particular kind of cutting equipment called a CO_2 laser cutter. This machine can engrave or cut a wide variety of materials. An description of how a CO_2 laser cutter operates, in its most basic form, is as follows:

Laser Generation

The CO_2 laser tube is the most important component of the CO_2 laser cutter. It is composed of a variety of gases, the most abundant of which are carbon dioxide, nitrogen, and helium, along with traces of other gases. The laser tube receives its energy supply from an electrical source, which causes the gas molecules to become excited and achieve a higher energy state.

Energy Amplification

The photons that are released as a result of the excited gas molecules being responsible for the emission of laser light. This primary laser beam is then directed through a number of mirrors and lenses, each of which contributes to the overall amplification and intensification of the beam.

Beam Delivery

After being amplified, the laser beam is sent to the cutting head in one of two ways: either by a series of mirrors or a beam delivery system. The usual component of this head is a focusing lens, which works to condense the laser beam into a comparatively tiny yet highly concentrated area.

Material Interaction

The surface of the material being cut is rapidly heated whenever the concentrated laser beam comes into contact with the material. The high energy density of the laser causes the material to evaporate or melt, which results in the creation of a thin line that can be cut or engraved. Depending on the characteristics of the material, the laser energy can either be absorbed by it or reflected by it.

CNC Control

A computer numerical control (CNC) system is what guides the movement of the cutting head on a laser cutter. The instructions for the intended cutting path are sent from the design software to the CNC system, which then accurately directs the cutting head along the path. This makes it possible to create precise and intricate cuts or engravings.

Auxiliary Systems

Cutting performance and safety are typically improved with the installation of supplementary systems in CO_2 laser cutters. These may include a ventilation system for removing fumes and smoke generated during cutting, a cooling system for maintaining the appropriate temperature of the laser tube, and safety measures such as protective enclosures and emergency stop buttons. Alternatively, these may be included within the laser cutting machine itself.

It is essential to keep in mind that CO_2 laser cutters are best utilized for cutting non-metallic materials such as wood, acrylic, plastics, and fabrics, in addition to some types of metals that have been coated with a suitable substance. Because these materials are able to effectively absorb the wavelength of the CO_2 laser (10.6 micrometers), cutting or engraving may be done quickly and easily.

Table 1. Table of Characteristics of the *CO_2* Laser Cutter Used

Workspace	70 cm x100 cm
Laser Type	CO_2 Glass Tube
Laser Power	Standart 80-100 W (Optional 60-80-100-130-150-180W)
Control Card	Ruida 6442
Movement System	-Step Motor - Linear guide rails and car
Scraping Speed	500mm/s
Sensitivity	0.05 mm/meter
Cooling	CW3000 (Water Cooled)
Energy Consumption	2 kWatt / hour
Electricity	AC 220VAC 50-60Hz Monophase
Machine Size	Width 153 cm x Length 110 cm x Height 120 cm
Weight	210 kg
Cuttable Materials	MDF, Plywood, Acrylic (Plexiglas), Wood, Leather, Vinlex, Jeans, Fabric types, Paper, Cardboard, Cardboard, Strofor, PVC, Dekota (forex)
Marked Materials	Painted metal surfaces, mirrored and transparent plexiglass, glass, mirrors, marble, ceramic, granite and its variants.
Connection	Network LAN + USB cable connection + USB external memory
Software	RD Works panel software + direct connection with Corel Draw, Auto CAD
Supported Formats	AI, DXF, PLT, DST, DSB, BMP, GIF, JPEG, PNG, MNG, TIFF, TGA, PCX, WBMP, WMF, EMF, JBG, JP2, PGX, RAS, PNM, SKA, RAW
Characteristics	Precise operation and smooth mechanical assembly with square slides and trolleys. Thanks to its divisible ergonomic design, it provides easy installation by using doors and entrances with 60cm passage area. In addition to air conditioner condenser gas supported water cooling, heating system is available. The Stop Start feature allows for the resumption of operations from the previous state in the event of power failure or similar incidents. The internal memory enables the storage of files directly on the motherboard, facilitating quick and direct start of the process. The 3.5-inch color TFT screen provides a visual interface to view saved files, monitor ongoing operations, track elapsed time, and make desired setting adjustments.Most efficient laser beam power thanks to imported US Znse focus lens and gold alloy silicon mirrors. Fully automatic cooling chiller + Air compressor + Air evacuation motor included in the price

Figure 3.1. CO_2 Laser Cutter

3.1.3. Syringe Pump

A syringe pump is a specialized device used for precise and controlled fluid delivery in various applications. It typically consists of a syringe, piston, valves, and a motor mechanism. The syringe serves as a reservoir for the fluid or gas to be dispensed, while the piston, connected to a motor, moves within the syringe barrel. By regulating the movement of the piston, syringe pumps can accurately control the flow rate and volume of the dispensed substance.

The working principle of a syringe pump revolves around the reciprocating motion of the piston within the syringe barrel. When the motor drives the piston forward, the volume within the syringe decreases, leading to the expulsion of the fluid or gas through an outlet. Conversely, when the piston moves backward, the syringe draws in a specific amount of fluid or gas. This cyclic motion of the piston enables precise dosing and control of the substance being delivered.

Syringe pumps have a wide range of applications across fields such as medicine, biotechnology, chemistry, and research laboratories. In medical settings, they are frequently employed for administering medication with accuracy and precision. Their ability to deliver fluids in controlled quantities makes them valuable in scientific experiments and analysis, where precise dosing and fluid control are crucial. Syringe pumps offer advantages like low dead volume, minimal pulsation, and compatibility with different types of syringes, making them versatile and reliable tools for fluid delivery in various industries.

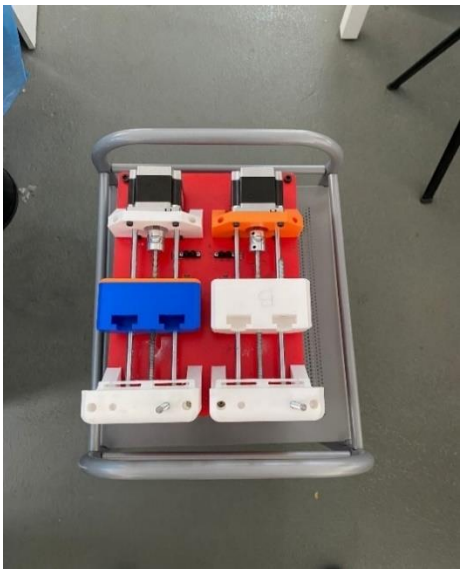

Figure 3.2. Syringe Pump Used In The Experiment

Figure 3.3. Interface Of The Program Flow Control İntegrated With The Syringe Pump Used

3.2. Device Fabrication and Operation

As can be seen in Figure 3.4., the microfluidic device is intended to feature a single inlet, a serpentine focusing section, and a spiral separation section with two exits. All three sections are connected by a spiral. Concerning the serpentine section, analogous designs found in the aforementioned body of research were taken into consideration with regard to the number and dimensions of the serpentines that produce appropriate particle focusing. The spiral portion was intended to contain three loops, and there was to be a suitable space between each loop. This was done in order to provide the necessary rigidity for the assembling process of the device. The three layers of the gadget were laser-cut, and the bottom and top layers were assembled using double-sided transparent tape manufactured by 3M in Minnesota, United States of America. In order to cut the PMMA, a typical 100W CO_2 laser plotter from Lazerfix in Konya, Turkey was utilized. The thickness of the bottom layer was 300 micrometers, the thickness of the middle layer was 100 micrometers, and the thickness of the top layer was 3 mm. It was decided that the top layer would be significantly thicker in order to give adequate depth for the inlet and outflow tubes.

When testing the device, polystyrene particles with sizes of 1 and 5 micrometers were utilized at concentrations of 107 and 3x107 particles per milliliter, respectively. In order to simulate the process of cell and bacteria separation, Saccharomyces cerevisiae yeast cells (at a concentration of around 107 cells/ml) and polystyrene particles with a size of 1 micrometer were utilized. A conventional hemocytometer was utilized for the purposes of characterizing the particle and cell counts. For the injection of the cell/particle solution, a home-built syringe pump system was utilized (Akkoyun & Ozcelik, 2020).

The photos were captured with a CMOS camera (HD, Euromex, Arnhem, Netherlands) and an in-verted microscope (OX.2053-PLPH, Euromex, Arnhem, Netherlands). To make the yeast growth medium, one liter of sterile distilled water was mixed with ten grams of yeast extract, twenty grams of peptone, and twenty grams of dextrose. This mixture was then stirred until it was completely dissolved. After inoculating 10 mL of growth media with Saccharomyces cerevisiae yeast culture, the mixture was heated to 30 degrees Celsius and gently shaken throughout the incubation process. After that, the yeast cells were extracted by centrifuging them at a speed of 4000 x g for five minutes. The yeast cells were

resuspended in 10 mL of sterile distilled water, and the super-natant was discarded after it had been collected.

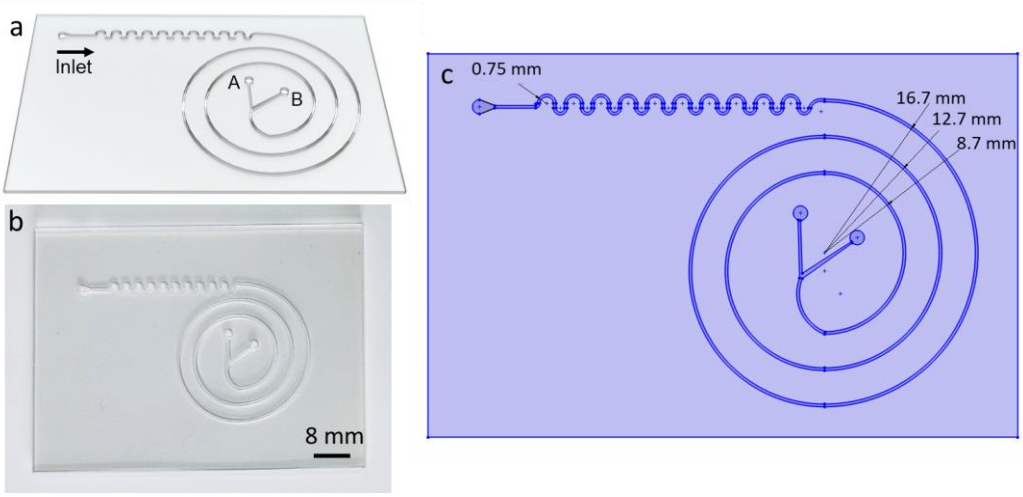

Figure 3.4. a) Schematic depiction, b) actual picture and c) dimensions of the device is shown.

3.3. Working Mechanism of the Device

The theory of inertial particle separation, commonly known as the Dean effect or Dean flow, provides an explanation for the behavior of particles of varying sizes as they move through a channel with a curvature. The amount of force exerted by Dean rises as the channel's size, curvature, and flow velocity all increase. Particles can be propelled towards the inner or outer wall of a microchannel depending on their size and the drag force that they encounter, which is created by Dean vortices. This movement can occur regardless of whether the microchannel is filled with fluid or not. Particles moving in a curvilinear channel are subject to a variety of forces, including those resulting from pressure and inertial lift. Particles have a propensity to assume equilibrium positions, which are those in which the various lift forces that impinge on them are balanced out to provide a net lift force. In addition, thin bands are formed by these equilibrium points. In serpentine channels, by making use of the inertial forces that act on the particles as they flow through the curved sections of the channel, it is possible to concentrate the flow of particles into a specific area. In particular, when a fluid that contains particles flows over a curved segment of the channel, inertial forces operate on the particles, causing them to move towards the outer wall based on their sizes. This movement is determined by the curvature of the channel. Because of the counteracting effects

of the hydrodynamic forces, the particles in the fluid do not migrate laterally as it enters a stretch of the channel that is horizontally straight. As a direct consequence of this, the particles move closer and closer to the channel's center. Particles can be continually focussed based on their size through the employment of a serpentine pattern that involves the arrangement of several curved and straight sections.

In the section of the channel that is shaped like a spiral, the dean flow, inertia forces, and drag forces are all balanced at precise positions in the channel for particles of varying sizes. It is common knowledge, gleaned from both the scientific literature and the inertial focusing observed in spiral channels, that larger particles travel closer to the inner wall of the microfluidic channel, while smaller particles are pushed toward the channel's outer wall. Before the particles enter the spiral microfluidic channels, the serpentine segment of the microfluidic channel that is utilised in this study is utilized to focus them at equilibrium points. In this manner, different diameter particles can be separated in the spiral channel without the need to use a sheath flow and with only a single input that is used for the injection of samples.

3.4. Numerical Analysis

In this section, general information about the simulation program used and some of the modules in the program will be given.

3.4.1. Finite Element Analysis and Finite Element Method

The abbreviations FEA and FEM stand for "Finite Element Analysis" and "Finite Element Method," respectively. They are frequently interchanged with one another due to their close relationship. The behavior of complex systems and structures can be analyzed using a method called finite element analysis (FEA), which is a type of numerical methodology. The structure is broken up into a series of progressively smaller and more elementary components, which are referred to as finite elements. After that, equations are solved in order to analyze the behavior of each component and how it interacts with the

components around it. After that, the behavior of the whole structure can be deduced from the behavior of these interconnected parts of the structure.

The continuous domain of a structure or system is broken up into discrete pieces, appropriate mathematical models and equations are applied to each element, and finally, the discrete elements are pieced together to provide a representation of the full structure or system. The finite element method (FEM) is a sophisticated numerical methodology that is frequently used in engineering and the applied sciences for the purpose of addressing complicated problems involving stress analysis, heat transfer, fluid movement, and a broad variety of other physical phenomena.

3.4.1.1. The Advantages of Using FEA and FEM

Design Optimization

Before actually building prototypes, engineers can optimize designs by simulating and analyzing numerous design configurations and variations thanks to finite element analysis (FEA). This aids in the identification of possible issues, the optimization of designs, and the reduction of expenses associated with development.

Prediction of Performance

Engineers are able to make accurate predictions regarding the behavior and performance of a structure or system under a variety of different operating situations by using finite element analysis (FEA). It provides assistance in measuring aspects like as stress, deformation, vibration, heat transfer, and fluid flow characteristics, all of which are essential for ensuring the structural integrity and performance of the structure.

Engineers are able to find and fix defects or weaknesses in the design more earlier in the development process when they use FEA. This helps them reduce costs. This assists in decreasing the chance of costly failures or rework further down the road, which ultimately leads to cost savings.

Efficiency in the Use of Time

In comparison to more conventional methods of analysis, FEA permits much quicker examinations. Powerful computers may be used to solve equations numerically, and complex

structures can be broken down into its component parts to make them more manageable. This drastically cuts down on the amount of time needed for analysis, allowing engineers to swiftly analyze a variety of different design options.

Testing in a Virtual Environment

FEA provides a testing environment in which engineers may simulate and analyze the performance of a structure or system without the requirement for actual prototypes. Virtual testing allows engineers to save time and money. This is especially useful in areas such as aerospace, automotive, and civil engineering, where conducting physical tests may be prohibitively expensive, time-consuming, or otherwise impossible.

Insight into Complicated processes

Finite element analysis (FEA) offers a comprehensive comprehension of the complicated physical processes that take place within a structure or system. It is helpful in visualizing and assessing aspects that are sometimes difficult or impossible to detect firsthand, such as stress concentrations, heat distribution, fluid flow pattern, and modal behavior. This can be accomplished through the use of computer simulations.

Overall, finite element analysis (FEA) and finite element modeling (FEM) are strong techniques that enable engineers to analyze, optimize, and forecast the behavior of structures and systems. This results in improved designs, lower costs, and faster development cycles.

3.4.2. Comsol Multiphysics

Users are able to model and simulate a broad variety of different physical occurrences with the help of the Comsol Multiphysics software package, which features both finite element analysis (FEA) and computational fluid dynamics (CFD). It is intended to be utilized in a wide variety of domains, such as electrical, mechanical, fluid, and chemical engineering, in addition to the fields of physics and biology.

The user is able to set up and solve difficult multiphysics problems with the help of the software's extensive variety of tools and features, which are included in their entirety. The graphical user interface (GUI) that is included in Comsol Multiphysics gives users the ability to configure and solve problems by making use of a variety of interactive tools and menus. A

programming interface is also included, which gives customers the ability to develop their own scripts and programs to automate and personalize the analysis process. When performing a comparison analysis, it is essential to take into careful consideration the input data and the assumptions that were used in the model, since it is crucial to keep in mind that the findings of a FEA analysis are only as accurate as the data and assumptions that were used in the model.

3.4.3. Laminar Flow

COMSOL Multiphysics is a robust software platform that gives users access to a wide variety of modules for the purpose of modeling and evaluating a wide variety of physical occurrences. The Laminar Flow Module is one of the modules that may be used with COMSOL Multiphysics. This module's primary focus is on modeling and analyzing laminar fluid flow.

Engineers and researchers can simulate and investigate the behavior of laminar flows using the Laminar Flow Module in COMSOL. Laminar flows are distinguished from other types of fluid motion by their smoothness and order, as well as by the presence of layers or streamlines.

The fundamental governing equations for laminar flow, such as the Navier-Stokes equations and the continuity equation, are incorporated into the module through its use of these equations. In the case of incompressible fluid flow, the conservation of mass and momentum can be described using these equations.

The Navier-Stokes equations are a set of partial differential equations that are used to explain the movement of fluid substances like liquids and gases. These equations were developed by Navier and Stokes. In the study of laminar flow, also known as smooth and orderly fluid motion with clearly defined layers or streamlines, these equations are utilized quite frequently. Smooth and organized fluid motion is referred to as laminar flow. The Navier-Stokes equations take into account the conservation of mass and momentum inside the fluid. The following is a detailed explanation of the Navier-Stokes equations:

Conservation of Mass

The first part of the Navier-Stokes equations is called the continuity equation, and it is essentially a statement about how mass should be conserved. It states that the rate of change of mass within a control volume is equal to the net mass flux across its boundaries. This is an important concept in the field of control volume analysis. The continuity equation can be expressed in mathematical terms as follows:

$$\frac{\partial \rho}{\partial t} + \nabla \cdot (\rho v) = 0 \qquad (7)$$

where ρ is the density of the fluid, t is time, v is the velocity vector, and $\nabla \cdot$ denotes the divergence operator.

Conservation of Momentum

In the Navier-Stokes equations, the concept of the conservation of momentum is represented by three different components: the x-component, the y-component, and the z-component. These equations establish a connection between the temporal rate of change in momentum and the forces that are exerted on the fluid.

The equation for the x-component, often known as the conservation of momentum in the x-direction, can be written as follows:

$$\rho\left(\frac{\partial v}{\partial t} + v \cdot \nabla v\right) = -\nabla P + \nabla \cdot \left(\mu(\nabla v + (\nabla v)^T)\right) + \rho g \quad (8)$$

where P is the pressure, μ is the dynamic viscosity of the fluid, and g is the acceleration due to gravity.

The y-component and z-component equations are similar, but with the appropriate component substitutions.

Simplified Form

When a fluid is supposed to have a laminar flow, the Reynolds number of the fluid is assumed to be low. This indicates that the viscous forces are more powerful than the inertial forces. Under this assumption, the convective term ($v \cdot \nabla v$) is typically negligible compared to other terms, resulting in a simplified form of the Navier-Stokes equations:

$$\rho\left(\frac{\partial v}{\partial t}\right) = -\nabla P + \nabla \cdot \left(\mu(\nabla v + (\nabla v)^T)\right) + \rho g \ (9)$$

Because it ignores the convective factor, this simplified form is frequently employed for the analysis of laminar flows. As a result, the mathematical solution to the equations is made easier by using this form.

Analytical solutions to the Navier-Stokes equations are difficult to achieve for the vast majority of real-world flow situations because they are part of a system of nonlinear partial differential equations. In order to come up with an approximation of the solutions and mimic the behavior of laminar flow in a variety of engineering applications, numerical methods such as finite element analysis and finite difference methods are frequently utilized.

Boundary Conditions

Different flow situations can be represented by a variety of boundary conditions, such as inlet velocity profiles, pressure conditions, and wall conditions. These boundary conditions can be described in a number of different ways. These conditions are absolutely necessary in order to accurately simulate the flow behavior of the real world.

Predefined Physics Interfaces

The Laminar Flow Module has predefined physics interfaces that make it possible for users to simulate particular categories of laminar flows. These categories include steady-state flows, transient flows, single-phase flows, multiphase flows, and flows that involve heat transfer. These interfaces offer a straightforward and intuitive method for the configuration of simulations.

Fluid Properties

COMSOL gives its users the ability to define fluid properties for a variety of fluids, such as the fluid's density, viscosity, and thermal conductivity. This permits the simulation of laminar flow for a variety of fluids, including liquids and gases, as well as other forms of fluids.

Mesh

In order to discretize the computational domain, the module provides customizable meshing capabilities. COMSOL offers a variety of meshing techniques, which allows for the precise representation of flow features and the efficient computation of those features.

Visualization and Post-processing

COMSOL Multiphysics has strong capabilities for visualization and post-processing of simulation results for analysis purposes. Users are able to see flow patterns, velocity profiles, pressure distributions, and other pertinent parameters through the use of this software. In addition, they have the ability to collect data, produce graphs, and carry out quantitative analysis in order to garner insights from the simulation's outcomes.

Multiphysics Coupling

The Laminar Flow Module in COMSOL Multiphysics can be coupled with other modules, such as the Heat Transfer Module or the Chemical Engineering Module, through the Multiphysics Coupling feature. This makes it possible to conduct a study of complicated multiphysics processes, such as the transmission of heat in fluid flows or chemical reactions in laminar flow systems.

Laminar fluid flow phenomena can be modeled, simulated, and analyzed with the help of COMSOL Multiphysics' Laminar Flow Module, which comes equipped with an extensive collection of tools and capabilities. In order to acquire insights into flow behavior and optimize designs, it is widely utilized in a variety of sectors and research fields, including mechanical engineering, chemical engineering, biomedical engineering, and microfluidics.

3.4.4. Particle Tracing for Fluid Flow

The COMSOL Multiphysics module known as Particle Tracing for Fluid Flow makes it possible to simulate the motion of particles as they are moving through fluid flows. It makes it possible to track and analyze individual particles as well as groups of particles that are located inside a flow field. An illustration of the notion is provided in the following example:

Consider a scenario involving a conduit through which water continuously flows. The objective is to analyze the behavior of particles suspended in the water and track their paths as they traverse the pipe. The following steps outline the general procedure for simulating this scenario using the Particle Tracing for Fluid Flow module in COMSOL Multiphysics:

Geometry and Mesh

Construct the geometry of the pipe and import it into COMSOL for analysis. Generate a mesh suitable for the computational domain.

Physics Settings

Define the mechanical properties of the fluid, such as density and viscosity, to establish the flow mechanics. Specify the flow conditions, including pressure boundary conditions or inlet velocity boundary conditions.

Particle Tracing Settings

For the simulation of fluid flow, turn on the particle tracking module. Size, mass, and beginning positions of the particles should be determined. It is possible to import particle distributions from external sources or specify the desired number of particles.

Particle-Fluid Interaction

Describe how the flow of fluid and the particles interact. Configuring drag forces, lift forces, and particle-particle interactions are examples of this. These interactions can be described using either specialized models or empirical correlations.

Solver and Time Stepping

Solver settings should be adjusted to include parameters such as the duration of each time step and convergence criteria. The choice between time-dependent simulations or steady-state simulations depends on the specific flow characteristics.

Results and Visualization

Carry out the simulation, and then have a look at the outcomes. Tools to view particle trajectories, follow their positions over time, and extract pertinent data such as particle concentration, residence duration, or collision statistics are provided by the Particle Tracing module.

The Particle Tracing for Fluid Flow module that is included in COMSOL Multiphysics provides a flexible framework for the investigation of the behavior and transport of particles in fluid flows. Applications can be found for it in a variety of sectors, such as environmental engineering, chemical engineering, the pharmaceutical industry, and research based on particles.

3.4.5. Meshing

A description of the mesh and the function it serves is as follows:

Discretization

The intricate geometry of a building or system is broken down into a collection of smaller pieces by the mesh. These building blocks can appear as triangles, quadrilaterals, or tetrahedra in two dimensions, or hexahedra or tetrahedra in three dimensions. Each element stands for a relatively insignificant fraction of the domain and is characterized by its own unique collection of nodes and shape functions.

Element Connectivity

The mesh links the nodes of neighboring elements, so determining their relationships and the ways in which they interact with one another. The information about the connection serves as the foundation for the process of solving the governing equations of the FEA/FEM analysis.

Numerical Approximation

Both finite element analysis and finite element modeling rely on numerical methods to solve the governing equations. A discretized representation of the domain is provided by the mesh, which makes it possible for the equations to be solved numerically on a limited number of elements and nodes. Next, in order to reach the answer, one must first establish an approximation of the behavior of the system or structure within each element.

Solution Accuracy

The quality of the mesh plays a significant role in determining how accurate the FEA/FEM analysis is. Important characteristics of the system being investigated can be more accurately captured by a mesh that has been carefully created and polished. A good mesh guarantees that the calculated results are more reliable and representative of the actual behavior by effectively resolving the geometry and physical phenomena, such as stress concentrations or boundary layers. This is accomplished by correctly resolving the geometry and physical phenomena.

Computational Efficiency

The amount of computational work required for an analysis is affected by factors such as the size and complexity of a mesh. While more detailed meshes that contain more elements produce more accurate results, they also need more time and processing resources to process. It is essential to strike a reasonable balance between accuracy and computing efficiency by adjusting the level of mesh refinement in accordance with the requirements of the analysis and the resources that are at one's disposal.

Adaptivity

In certain circumstances, adaptive meshing strategies are utilized in order to accomplish the goal of bettering the analysis. Adaptive methods of mesh refinement or coarsening alter the mesh dynamically during the analysis based on particular criteria or error indicators. Because of this, the mesh is able to concentrate elements in regions of interest or refine areas with strong gradients, which simultaneously improves accuracy and maintains efficiency.

In a nutshell, the discretization of the domain into more manageable pieces is what the FEA and FEM analyses refer to as the mesh. In order to solve the governing equations, it offers a numerical approximation as well as connectivity. While the accuracy and reliability of the analysis results are directly impacted by the quality and refinement of the mesh, computing efficiency is another important factor that must be taken into consideration. It is impossible to gain meaningful insights into the behavior of structures and systems using FEA and FEM without first properly designing and refining the mesh used in the analysis.

Simulations using finite element analysis (FEA) and the finite element method (FEM) can benefit from meshing in a number of ways due to the fact that meshing is essentially the process of splitting a complicated geometry into smaller parts. The following is a list of the primary advantages of meshing:

Accuracy

A structure or system being investigated can have its geometry, boundaries, and features faithfully represented by a mesh that has been carefully created. The mesh guarantees that the calculated results are more precise and representative of the actual behavior by adequately resolving essential details such as stress concentrations, sharp corners, or

boundary layers. This is achieved by ensuring that the mesh effectively resolves critical details.

Solution Convergence

During the process of finding a solution, obtaining convergence with the use of an improved mesh is helpful. When the calculated solution converges, it signifies that it has reached a stable and consistent state. This ensures that additional refinement of the mesh will not significantly influence the results. The convergence behavior of the analysis is improved when a mesh has been modified appropriately, which makes the analysis more dependable.

Resolution of Local Phenomena

Localized areas of the domain being investigated are frequently the sites of occurrence for physically complex events. The use of a tiny mesh makes it possible to record such local events, which in turn makes it possible to conduct an exact examination of factors such as stress concentrations, fluid flow separation, or heat transfer gradients. The resolution of these local effects enables the mesh to provide in-depth insights into essential facets of the system.

Efficient Resource Utilization

The process of mesh refinement should strive to achieve a balance that satisfies both the needs for accuracy and those for the most efficient use of computational resources. If the mesh is too coarse, it is possible that crucial information will be missed, which could lead to inaccurate findings. On the other side, if the mesh is too refined, it may increase the amount of computing that is necessary. Through careful and painstaking construction of the mesh, engineers are able to achieve a satisfactory balance. Because of this, they are able to make the most efficient use of the computational resources at their disposal without compromising the accuracy of their results.

Adaptivity

The benefits of meshing can be further improved with the application of adaptive meshing techniques. These methods involve dynamically refining or coarsening the mesh throughout the analysis based on specified criteria or error indications. This can be done either by increasing or decreasing the number of cells in the mesh. The ability to allocate computational resources to the locations in which they are required the most is made possible by adaptive meshing, which simultaneously improves accuracy and efficiency

Design Optimization

In the field of design optimization studies, meshing plays an essential part. Engineers are able to rapidly explore a variety of designs and configurations because to the ability to modify the mesh parameters. Some of these parameters include element sizes and element kinds. The flexibility of the meshing enables optimization algorithms to make adjustments to the mesh as necessary during the iterative process of design optimization, which ultimately results in improved designs.

Visualization and Post-processing

The viewing and post-processing of the data are both made easier by a mesh that has been well-structured. As a result, engineers are better able to understand parameters such as stress contours, temperature distributions, or fluid flow patterns. This makes it possible to clearly portray the system being investigated. In addition, the facilitation of the extraction of usable data for the purpose of additional analysis or comparisons is provided by a model that has been well-meshed.

In conclusion, meshing offers a wide variety of advantages to the simulations of FEA and FEM. Accuracy, convergence, and the capacity to resolve local phenomena are all improved as a result of this. Engineers are able to effectively employ computing resources, execute design optimization, and gain clear visualization and post-processing results when they optimize the mesh and use adaptive approaches.

3.4.6. Studies

The term "studies" is utilized in COMSOL Multiphysics to refer to the different simulation scenarios and analyses that can be performed on a model. These studies enable the analysis of various aspects of the model and the exploration of parameters, boundary conditions, and physics settings. The following is a list of common types of studies available in COMSOL Multiphysics:

Parametric Sweep

This study allows for the adjustment of one or more model parameters within specified limits. By automatically conducting multiple simulations and systematically varying the

parameter values, COMSOL generates parametric plots or tables that illustrate how the model's output varies with different parameter values. It can be used for sensitivity analysis, optimization, or design space exploration.

Time-dependent Study

When modeling transient phenomena or dynamic behavior over time, this study is appropriate. It enables investigation into how the model responds to changes occurring over a specific time period, such as temperature or pressure variations. The time step size and total simulation time can be specified to capture the temporal behavior of the system.

Frequency Domain Study

For models exhibiting periodic or harmonic activity, the frequency domain study is useful. It allows for analysis of the model's response in the frequency domain, providing insights into natural frequencies, resonances, and frequency-dependent behavior. Users can specify a frequency range or individual frequencies of interest, and COMSOL conducts simulations to obtain the frequency response.

Eigenfrequency Study

This study focuses on determining the eigenmodes or inherent frequencies of the model. It is valuable for analyzing vibration modes, structural resonances, or acoustic modes. COMSOL computes the eigenvalues, eigenvectors, mode shapes, and corresponding frequencies of the system.

Optimization Study

With this study, users can optimize the design or parameters of a model based on specific criteria or goals. Design variables, constraints, and optimization targets can be defined. COMSOL runs multiple simulations, adjusting the design factors to find the best possible solution that meets the specified goals.

Stationary Study

This study is suitable for simulations involving steady states, where the system has reached a state of stable equilibrium. It is commonly used for analyzing static or quasi-static phenomena, such as thermal steady state, structural statics, or electrostatics. The governing equations are solved until a steady solution is reached.

These examples represent only a subset of the studies available in COMSOL Multiphysics. Each study type offers unique features and tools tailored to specific analysis requirements. By utilizing the various types of studies, users can conduct comprehensive investigations, gain new insights, and make well-informed decisions based on simulation results.

4. RESULTS AND DISCUSSIONS

In order to ascertain the behavior of particles while they were contained within the device and evaluate how effective the separation was, the laboratory studies relied on measurements that were taken in the live system. On the other hand, COMSOL simulations proved to be an invaluable tool for analyzing the intricate flow dynamics of the two spiral structures that were incorporated into the design of the device. This was done with the intention of improving the device's capacity for induction and particle separation.

The simulations revealed a discernible distinction, with larger particles approaching the inner walls and smaller particles settling near the outside walls. This was proved by the simulations. These results demonstrate that the suggested microfluidic device has the capability of performing selective manipulation based on the sizes of the particles. The knowledge that was gleaned from the laboratory experiments and the COMSOL simulations was extremely helpful in gaining insight into the physical mechanisms that lie beneath the observed behavior and in maximizing the efficiency of the design of microfluidic devices for use in applications involving particle separation.

4.1. Laboratory Results

At a range of different flow rates, polystyrene particles with sizes ranging from 1 to 5 micrometers was injected into the microfluidic device. The streak images that were collected from the device's entrance, the end of the serpentine section, and the exit of the spiral section are displayed in Figure 4.1.. This figure was created using an input flow rate of one thousand microliters per minute. At the beginning of the device, it can be seen that the polystyrene particles enter in a manner that results in a random distribution across the breadth of the channel (Figure 4.1.b). At the conclusion of the serpentine portion, polystyrene particles appeared to be forming a focussed stream that was visible to the naked eye (Figure 4.1.c). This is consistent with the findings that have been reported in the scientific literature for devices with comparable geometries (Javi et al., 2022; Amani et al., 2022; Zhang et al., 2014).

This focusing behavior is meant to be employed before the spiral channel in order to remove the necessity for a hydrodynamic flow focusing, which would require numerous inlets and sheath flow. This focusing behavior can be thought of as an alternative to the hydrodynamic flow focusing. Following the serpentine section of the microfluidic device, the particles that have been focused proceed to the spiral section, where they will be directed towards different streams according to the diameters of those streams (Figure 4.1.d). A darker stream can be seen approaching the inner wall, which is predominantly composed of particles measuring 5 µm.

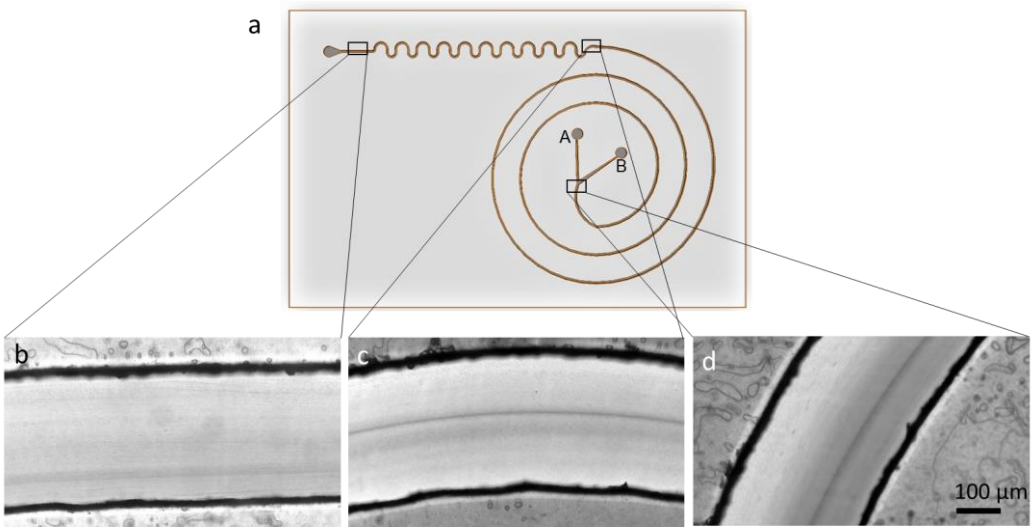

Figure 4.1. Particle focusing behavior is demonstrated using the combined device. a) Device schematic outline and image collection regions are shown. Streak images of particle flows are formed from b) entrance, c) exit of the serpentine section and d) exit of the spiral section

The effectiveness of the device in separating particles was evaluated quantitatively by subjecting it to a series of different inlet flow rates and then analyzing the particles that were collected from outlets A and B. It was discovered that inlet flow rates ranging from 600 µl/min to 1000 µl/min led to significantly higher levels of separation purity and efficiency. A sample of particle photographs is presented in Figure 4.2 at an inlet flow rate of 1000 µl/min. It is evident that the outlet A was used by the vast majority of the polystyrene particles with a size of 1 m, whereas the outlet B was used by the majority of the polystyrene particles with a size of 5µm.

This is an expected effect based on the predictions from the inertial focusing behavior of larger particles in the spiral microfluidic channels, which is also in keeping with the literature. This is an outcome that has been predicted to take place.

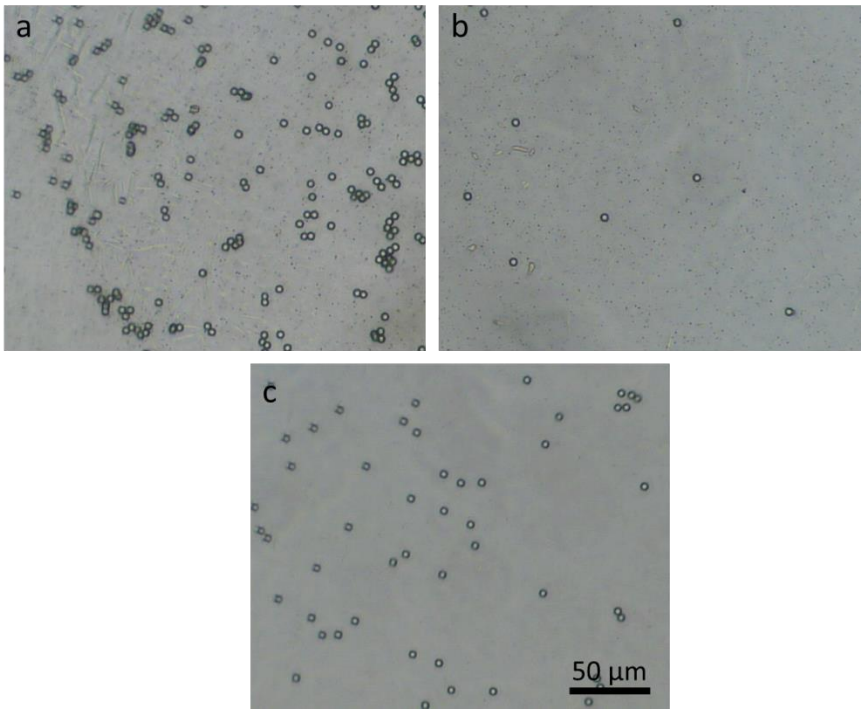

Figure 4.2. a) The mixture of 1 and 5 µm polystyrene particles before entering the device. Particles collected from b) the outlet A and c) the outlet B are shown.

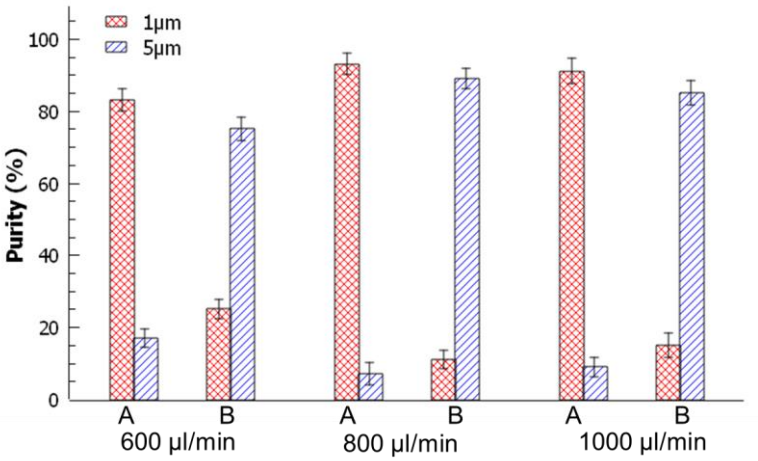

Figure 4.3. Purity of the particles collected from the outlets A and B at different flow rates. Error bars represent standard deviation of 5 different measurements.

Following that, the numbers of the collected particles were quantified using a hemocytometer counting the standard. The levels of purity of the samples that were gathered from outlets A and B are displayed in Figure 4.3. In this case, purity is determined by counting the number of polystyrene particles ranging from 1 to 5 µm micrometers in size that were collected from each outlet and then determining the ratio of those particles.

After experimenting with a variety of inlet flow rates, the purities were found to be enhanced at 600, 800, and 1000 µl/min. For the design of this device, it was discovered that the optimal performance in terms of the purity of the collected particles could be attained at a flow rate of 800 µl/min. The purities of particles with a size of 1 and 5 µm micrometers were found to be 93% and 89%, respectively, for outlets A and B. It was discovered that the contamination of outlet B by particles 1 micron in size was significantly higher than the contamination of outlet A by particles 5 microns in size. This is because the particles with a size of 1 µm have a greater degree of dispersion than those with a size of 5 µm , which are much larger. The inertial and dean fluxes concentrate their effects more strongly on the larger particles. The effectiveness of the particle separation procedure can also be determined using the samples that were collected. The ratio of the number of collected targeted particles to the overall number of target particles will be used to define "efficiency" for the purposes of this discussion. The separation efficiencies at 1 and 5 m were found to be 89% and 93%, respectively. Due to their larger size and superior focusing behavior, the majority of the particles with a size of 5 m were collected from the outlet that was designed for their collection.

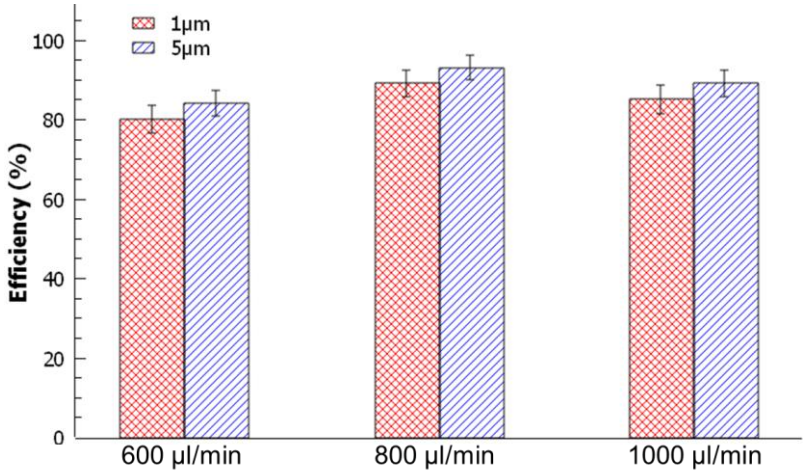

Figure 4.3. Separation efficiency for 1 and 5 µm polystyrene particles collected at different flow rates. Error bars represent standard deviation of 5 different measurements.

In the last step of the process, yeast cells and particles measuring 1 µm are separated using the apparatus to model the separation of bacteria and cells required for cell therapy applications. Yeast cells were selected for this project because they can be grown and kept alive in a typical laboratory setting with little effort and illustrate the physical features of living organisms. Since polystyrene particles with a size of 1 µm are quite near to the size of the majority of bacteria, these particles are employed to portray bacteria. The mixture of yeast cells and yeast particles is depicted in Figure 4.5.a before the cells and particles are separated. The samples that were collected from Outlet A and Outlet B are shown in Figure 4.5.b and Figure 4.5.c, respectively. In Figure 4.5.d, the purities of yeast cells and particles with a size of 1 µm after separation are given as 91% and 85% respectively. In comparison to the 5 µm particles, yeast cells produced a product with a lower purity because they were less homogeneous and exhibited greater variation in size. Also discovered were separation efficiency of 85% for yeast cells and 88% for particles measuring 1 µm, with the yeast cells coming out on top.

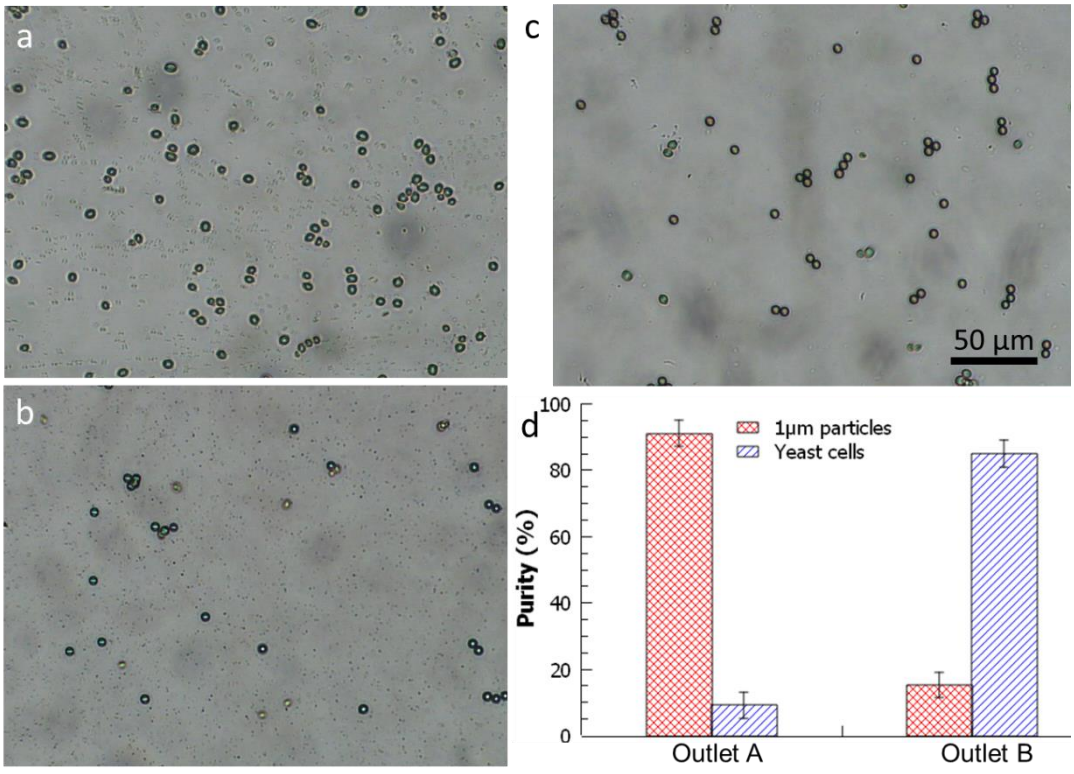

Figure 4.5. Separation of yeast cells and 1 µm particles. A) Cell and particle mixture before separation. B) sample collected from the outlet A. C) Sample collected from the outlet B. D) Purity of samples collected from the outlets A and B. Error bars represent standard deviation of 5 different measurements.

4.2. Simulation

In this section, results, and discussion of the COMSOL simulations conducted to investigate the particle separation performance of the proposed microfluidic device utilizing a two revolution geometry. The simulations aimed to provide insights into the behavior of particles within the device, their trajectories, and the efficiency of separation. By leveraging the computational capabilities of COMSOL, able to model and analyze the intricate fluid dynamics and particle interactions within the two revolution geometry, complementing the experimental laboratory tests previously conducted. The simulations were conducted under carefully selected input conditions, taking into account relevant parameters such as flow rates and particle properties. This section, present the simulation setup, methodology, and discuss the obtained results, providing a comprehensive analysis of the particle separation performance and insights into the underlying physical mechanisms driving the observed behavior.

4.2.1. Geometry:

The microfluidic device utilized in the COMSOL simulations features a well-defined geometry designed to enable efficient particle separation. The device consists of a rectangular channel with a width of 1000 μm and a height of 500 μm, providing sufficient space for fluid flow and particle manipulation. The channel incorporates two spiral structures, meticulously designed using CAD software, with each spiral spanning two complete revolutions. The spiral geometry was chosen to induce complex fluid dynamics, facilitating effective particle separation through the application of centrifugal and inertial forces. The dimensions and shape of the spirals were carefully optimized to ensure optimal particle trajectory manipulation and enhance separation performance. The device incorporates two input ports and two output ports, strategically positioned at opposite ends of the channel, allowing controlled injection and collection of fluid samples. The geometry of the microfluidic device was meticulously engineered to strike a balance between structural integrity, fluid flow characteristics, and efficient particle separation. The inputs are from the inner side of the geometry and outputs lies on the outward side of the geometry.

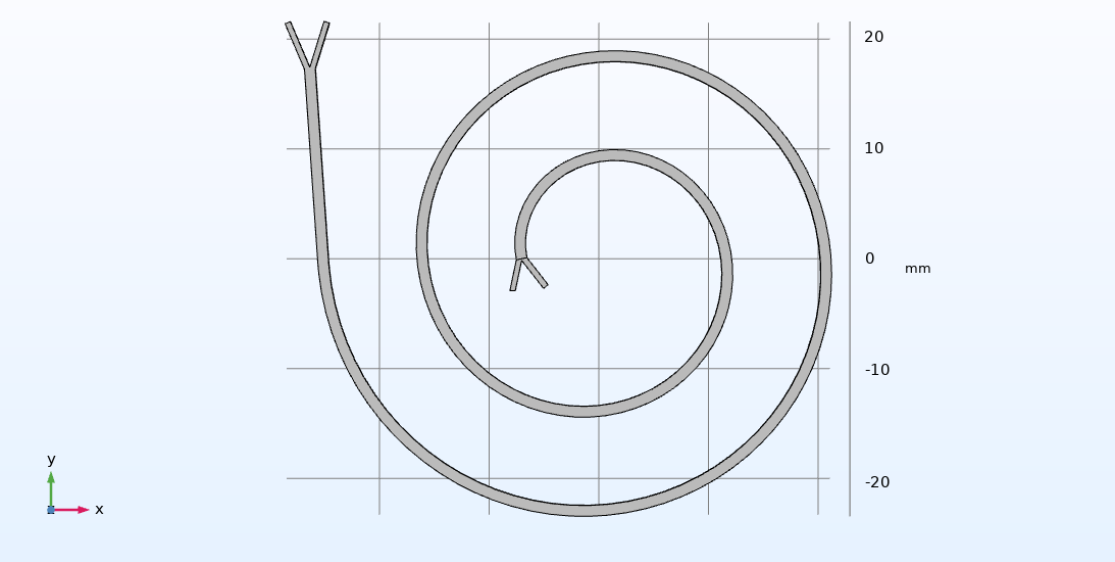

Figure 4.6. Geometry Created For Numerical Analysis

4.2.2. Boundary Conditions

To accurately simulate the fluid flow and particle separation within the microfluidic device, laminar flow analysis was employed in COMSOL to calculate the velocity fields. The main input velocity considered for the analysis was set at 0.45 m/s, representing the flow rate of the fluid within the device. The no-slip wall condition with a bounce boundary condition was applied to the channel walls. The bounce boundary condition allows the particles to interact with the walls by reflecting their velocities upon collision, mimicking the behavior of real microfluidic systems.

To evaluate the particle separation efficiency, the 'Particle Tracing for Fluid Flow' module in COMSOL was utilized. This module enables the tracing of particles within the simulated fluid flow, allowing for the assessment of their trajectories and separation behavior. In this module, two particles were injected into the system simultaneously, each with a distinct diameter but the same density of 1100 kg/m^3. Specifically, particles with diameters of 1 μm and 5 μm were selected to represent a range of particle sizes commonly encountered in particle separation applications.

To account for the forces acting on the particles, both drag force and lift force were considered in the particle tracing simulations. The drag force accounts for the resistance

experienced by the particles due to the fluid flow, while the lift force captures the effect of fluid vorticity on the particles. These forces were applied to the particles during their movement within the channel, influencing their trajectories and separation behavior.

By combining the calculated velocity fields, the no-slip wall condition with a bounce boundary condition, and the particle tracing methodology, the simulations enabled the visualization and analysis of the particle trajectories, thus providing insights into the effectiveness of the two-spiral geometry in separating particles of different sizes. The simulations facilitated the exploration of the complex interplay between fluid flow, particle dynamics, and the underlying separation mechanisms, shedding light on the separation efficiency achieved by the microfluidic device.

4.2.3. Analysis Results

The analysis using the laminar flow module in COMSOL provided valuable insights into the stationary velocity fields within the microfluidic device. By utilizing a slice plane, we were able to extract and visualize the velocity profiles along specific sections of interest within the channel. The resulting velocity graph, shown in Figure 4.7., depicts the magnitude of the stationary fluid velocity as a function of the position within the channel. The slice plane provides a cross-sectional view of the velocity field inside the channel, allowing us to observe the variations in velocity along different regions. The legends accompanying the graph provide a color scale that represents the magnitude of the fluid velocity, with warmer colors indicating higher velocities and cooler colors indicating lower velocities. The velocity graph highlights the controlled and directed fluid flow induced by the two-spiral geometry, with higher velocities observed near the center of the spirals and relatively lower velocities near the channel walls. This stationary analysis is crucial for understanding the steady-state fluid dynamics within the microfluidic device and its implications for particle manipulation and separation.

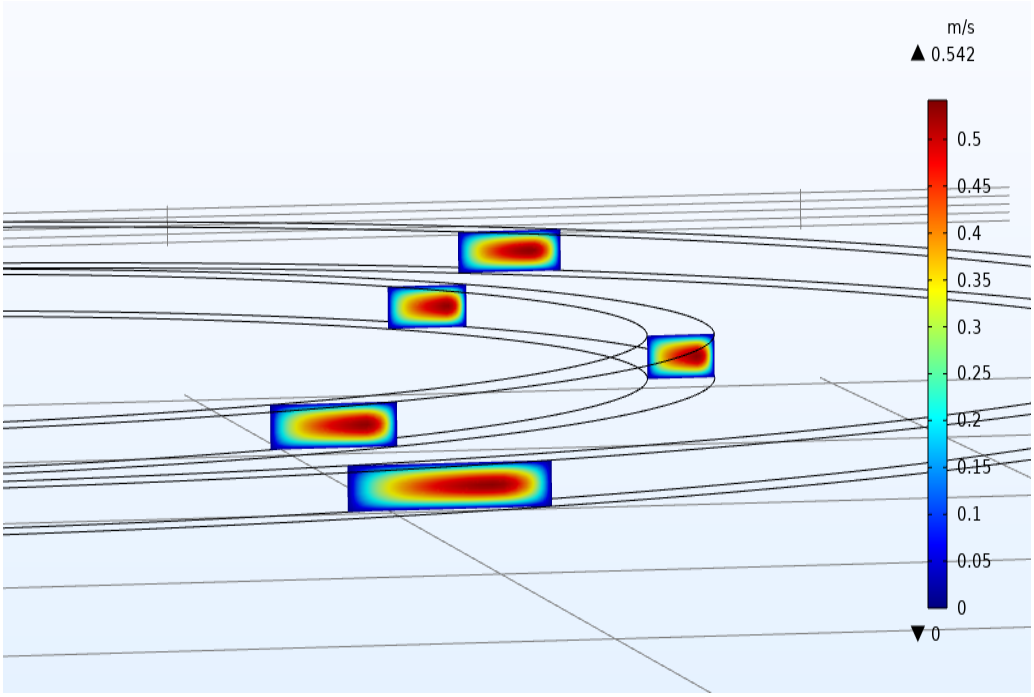

Figure 4.7. Velocity Fields İnside The Channel

The behavior of particles inside the microfluidic device was simulated using COMSOL's Particle Tracing for Fluid Flow module. The models took into account how the particles would respond to both lift and drag forces. The drag force, proportional to the particle size, acted to retard the motion of particles in the fluid flow, while the lift force, arising from fluid vorticity, induced lateral displacements. As a result, larger particles experienced stronger drag forces and tended to move towards the inner walls of the device, while smaller particles exhibited relatively less influence from the lift force and were positioned closer to the outer walls.

At the outlet of the microfluidic device, clear separation between the particles was observed, as depicted in Figure 4.8.. The figure showcases the distinct arrangement of particles, with the larger particles concentrated towards the inner walls and the smaller particles occupying the outer region. The separation achieved through the two-spiral geometry demonstrates the effectiveness of the microfluidic device in selectively manipulating particles based on their sizes. To aid in the interpretation of the Figure 4.8., a diameter legend is provided, allowing for a visual correlation between the particle size and its spatial distribution within the microfluidic device.

The particle tracing simulations provided valuable insights into the separation behavior, confirming the capability of the proposed microfluidic device to effectively separate particles based on their sizes. This information is crucial for understanding the underlying physical mechanisms and optimizing the design of microfluidic devices for particle separation applications.

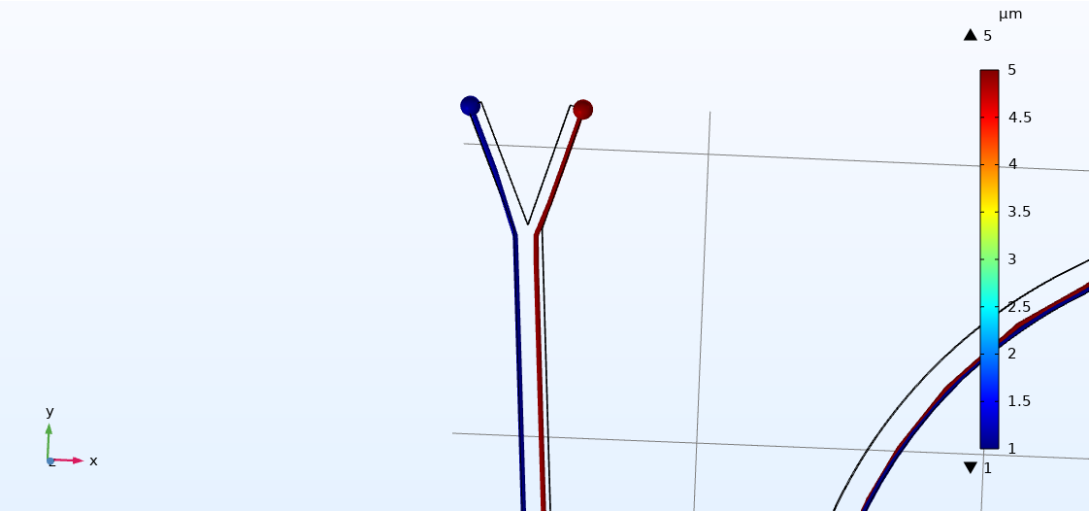

Figure 4.8. Particle Separation at The Outlet

The discussion of the COMSOL simulations focuses on the results obtained and their implications for the particle separation performance of the proposed microfluidic device. The simulations provided valuable insights into the behavior of particles within the device, their trajectories, and the efficiency of separation.

The geometry of the microfluidic device, featuring a rectangular channel with two spiral structures spanning two complete revolutions, was carefully designed to induce complex fluid dynamics and enhance particle separation. The simulations showcased the controlled and directed fluid flow induced by the two-spiral geometry, with higher velocities observed near the center of the spirals and relatively lower velocities near the channel walls. This steady-state fluid dynamics is crucial for effective particle manipulation and separation.

The particle tracing simulations demonstrated the effectiveness of the microfluidic device in separating particles based on their sizes. The smaller particles showed less influence from the lift force and were located closer to the outer walls, whereas the larger particles encountered stronger drag forces and tended to concentrate towards the inside walls of the device.

There was a distinct separation of the particles at the microfluidic device's outflow, with the smaller particles occupying the outside region and the larger particles being concentrated along the interior walls.

These results indicate that the proposed microfluidic device utilizing the two-spiral geometry is capable of selectively manipulating particles based on their sizes. The complex interplay between fluid flow, particle dynamics, and the applied centrifugal and inertial forces contributes to the achieved separation efficiency. The insights gained from the simulations provide valuable information for understanding the underlying physical mechanisms and optimizing the design of microfluidic devices for particle separation applications.

It is important to note that the simulations complemented the experimental laboratory tests previously conducted, providing a deeper understanding of the device's performance. The computational capabilities of COMSOL allowed for the modeling and analysis of intricate fluid dynamics and particle interactions within the two revolution geometry, contributing to the comprehensive analysis of the particle separation performance.

In conclusion, the COMSOL simulations provided valuable insights into the behavior of particles within the proposed microfluidic device and confirmed its capability to effectively separate particles based on their sizes. The results contribute to the understanding of the underlying physical mechanisms driving the observed behavior and provide guidance for the optimization of microfluidic devices for particle separation applications. Future research can further explore different geometries, input conditions, and particle properties to enhance the performance of such devices.

5. CONCLUSION

In conclusion, the data obtained from the laboratory experiment and COMSOL simulations provided useful information on the performance of the 2 different proposed microfluidic devices in terms of particle separation. The COMSOL simulations provided further insight into the underlying fluid dynamics and particle interactions within the two-helix geometry. The laboratory experiment proved that the device is successful in selectively managing particles based on their size.

The laboratory experiment demonstrated successful separation of polystyrene particles ranging from 1 μm to 5 μm in diameter. Photographs of streaks obtained at various points along the microfluidic device showed a transition from a random distribution of particles at the inlet of the device to a focused flow within the serpentine section resulting in a clear separation within the spiral zone. This progression is emphasized by the images of the lines. The purity and efficiency of the separation achieved at various flow rates provided additional evidence that the device is indeed capable of particle separation.

The findings from the experiments were supported by simulations performed in COMSOL, which provided a detailed study of the fluid flow and particle behavior occurring inside the microfluidic device. The simulations showed that the two spiral shapes control and direct the fluid flow, with higher velocities towards the center of the spirals and lower velocities near the channel walls. Particle tracking simulations showed that particles are successfully separated by size, with larger particles concentrated closer to the inner walls and smaller particles positioning themselves closer to the outer walls.

The combination of these findings sheds light on the complex relationship that exists between the dynamics of the fluid, the dynamics of the particles and the applied forces within the microfluidic device. The integration of experimental and computational methods provides a better understanding of the underlying physical mechanisms responsible for the execution of the particle separation process.

The successful use and analysis of 2 different geometric shapes used in laboratory experiments and COMSOL simulations has been shown to have accurate particle manipulation and separation capability. The findings provide evidence that two different spiral shapes are a successful method to achieve selective separation. This opens the door to potential applications in various sectors, including biology, biotechnology and medical diagnostics.

Overall, the findings of this research contribute to the development of microfluidic-based approaches for the separation of particles and provide useful information for the design and optimization of microfluidic devices. Our capacity to design particle separation methods that are both efficient and accurate and can be applied in a wide variety of contexts is enhanced when we combine experimental and computational approaches.

REFERENCES

Amani, A. M., Shamloo, A., Vatani, P., & Ebrahimi, S. (2022). Particles Focusing and Separation by a Novel Inertial Microfluidic Device: Divergent Serpentine Microchannel. Industrial & Engineering Chemistry Research, 61(38), 14324–14333. https://doi.org/10.1021/acs.iecr.2c02451

Ashkin, A., & Dziedzic, J. M. (1987). Optical Trapping and Manipulation of Viruses and Bacteria. *Science*, *235*(4795), 1517–1520. https://doi.org/10.1126/science.3547653

Asmolov, E. S. (1999). The inertial lift on a spherical particle in a plane Poiseuille flow at large channel Reynolds number. *Journal of Fluid Mechanics*, *381*, 63–87. https://doi.org/10.1017/s0022112098003474

Autebert, J., Coudert, B., Bidard, F., Pierga, J., Descroix, S., Malaquin, L., & Viovy, J. (2012). Microfluidic: An innovative tool for efficient cell sorting. *Methods*, *57*(3), 297–307. https://doi.org/10.1016/j.ymeth.2012.07.002

Bayareh, M., & Mortazavi, S. (2009). Numerical simulation of the motion of a single drop in a shear flow at finite Reynolds numbers. Iranian Journal of Science and Technology Transaction B, Engineering, 33(B5), 441-452.

Bayareh, M., & Mortazavi, S. (2011). Binary collision of drops in simple shear flow at finite Reynolds numbers: Geometry and viscosity ratio effects. *Advances in Engineering Software*, *42*(8), 604–611. https://doi.org/10.1016/j.advengsoft.2011.04.010

Bhagat, A. a. S., Bow, H., Hou, H. W., Tan, S. T., Han, J., & Lim, C. T. (2010). Microfluidics for cell separation. *Medical & Biological Engineering & Computing*, *48*(10), 999–1014. https://doi.org/10.1007/s11517-010-0611-4

Blankenstein, G. & Technical University of Denmark. (1998). *A micro flow system for particle separation and analysis*. https://patents.google.com/patent/WO1998010267A1/en

Bonner, W., Hulett, H. R., Sweet, R., & Herzenberg, L. A. (1972). Fluorescence Activated Cell Sorting. *Review of Scientific Instruments*, *43*(3), 404–409. https://doi.org/10.1063/1.1685647

Cho, S. W., Chen, C., Tsai, F. T., Godin, J., & Lo, Y. (2010). Human mammalian cell sorting using a highly integrated micro-fabricated fluorescence-activated cell sorter (μFACS). *Lab on a Chip*, *10*(12), 1567. https://doi.org/10.1039/c000136h

Coşkuner, E. (2014). *Mikroakışkan Sistemlerin Tasarımı, Üretimi ve Partikül Ayrıştırma Karakterizasyonu* [Master's Thesis]. Istanbul Teknik Universitesi.

Evander, M., Johansson, L., Lilliehorn, T., Piškur, J., Lindvall, M., Johansson, S., Almqvist, M., Laurell, T., & Nilsson, J. (2007). Noninvasive Acoustic Cell Trapping in a Microfluidic Perfusion System for Online Bioassays. *Analytical Chemistry*, *79*(7), 2984–2991. https://doi.org/10.1021/ac061576v

Fung, Y. (1973). Stochastic flow in capillary blood vessels. *Microvascular Research*, *5*(1), 34–48. https://doi.org/10.1016/s0026-2862(73)80005-6

Guan, G., Wu, L., Bhagat, A. a. S., Li, Z., Chen, P., Chao, S., Ong, C. J., & Han, J. (2013). Spiral microchannel with rectangular and trapezoidal cross-sections for size based particle separation. Scientific Reports, 3(1). https://doi.org/10.1038/srep01475

Han, K., & Frazier, A. B. (2004). Continuous magnetophoretic separation of blood cells in microdevice format. *Journal of Applied Physics*, *96*(10), 5797–5802. https://doi.org/10.1063/1.1803628

Herzenberg, L. A., Sweet, R. G., & Herzenberg, L. A. (1976). Fluorescence-Activated Cell Sorting. *Scientific American*, *234*(3), 108–117. https://doi.org/10.1038/scientificamerican0376-108

Hood, K., Lee, S., & Roper, M. (2013). Inertial migration of a rigid sphere in three-dimensional Poiseuille flow. *Journal of Fluid Mechanics*, *765*, 452–479. https://doi.org/10.1017/jfm.2014.739

Huang, L. R., Cox, E. C., Austin, R. H., & Sturm, J. C. (2004). Continuous Particle Separation Through Deterministic Lateral Displacement. *Science*, *304*(5673), 987–990. https://doi.org/10.1126/science.1094567

Hulett, H. R., Bonner, W., Barrett, J. R., & Herzenberg, L. A. (1969). Cell Sorting: Automated Separation of Mammalian Cells as a Function of Intracellular Fluorescence. *Science*, *166*(3906), 747–749. https://doi.org/10.1126/science.166.3906.747

Jackson, E. L., & Lu, H. (2013). Advances in microfluidic cell separation and manipulation. *Current Opinion in Chemical Engineering*, *2*(4), 398–404. https://doi.org/10.1016/j.coche.2013.10.001

Jäggi, R. D., Sandoz, R., & Effenhauser, C. (2006). Microfluidic depletion of red blood cells from whole blood in high-aspect-ratio microchannels. *Microfluidics and Nanofluidics*, *3*(1), 47–53. https://doi.org/10.1007/s10404-006-0104-9

Javi, F., Zaferani, M., Lopez-Barbosa, N., DeLisa, M. P., & Abbaspourrad, A. (2022). Sheathless inertial microfluidic cell separation via a serpentine–contraction–expansion device coupled with a combinatorial extraction regulator. *Microfluidics and Nanofluidics*, *26*(7). https://doi.org/10.1007/s10404-022-02559-7

Jiménez, N., Groby, J., & Romero-García, V. (2021). Spiral sound-diffusing metasurfaces based on holographic vortices. Scientific Reports, 11(1). https://doi.org/10.1038/s41598-021-89487-8

Joensson, H. N., Uhlén, M., & Svahn, H. A. (2011). Droplet size based separation by deterministic lateral displacement—separating droplets by cell-induced shrinking. *Lab on a Chip*, *11*(7), 1305. https://doi.org/10.1039/c0lc00688b

Johansson, L., Nikolajeff, F., Johansson, S., & Thorslund, S. (2009). On-Chip Fluorescence-Activated Cell Sorting by an Integrated Miniaturized Ultrasonic Transducer. *Analytical Chemistry*, *81*(13), 5188–5196. https://doi.org/10.1021/ac802681r

Kim, Y., & Yoo, J. U. (2008). The lateral migration of neutrally-buoyant spheres transported through square microchannels. *Journal of Micromechanics and Microengineering*, *18*(6), 065015. https://doi.org/10.1088/0960-1317/18/6/065015

Laurell, T., Petersson, F., & Nilsson, A. (2007). Chip integrated strategies for acoustic separation and manipulation of cells and particles. *Chemical Society Reviews*, *36*(3), 492–506. https://doi.org/10.1039/b601326k

Larsen, A. V., Poulsen, L., Birgens, H., Dufva, M., & Kristensen, A. (2008). Pinched flow fractionation devices for detection of single nucleotide polymorphisms. *Lab on a Chip*, *8*(5), 818. https://doi.org/10.1039/b802268b

Lewpiriyawong, N., Kandaswamy, K., Yang, C., Ivanov, V., & Stocker, R. (2011). Microfluidic Characterization and Continuous Separation of Cells and Particles Using Conducting Poly(dimethyl siloxane) Electrode Induced Alternating Current-Dielectrophoresis. *Analytical Chemistry*, *83*(24), 9579–9585. https://doi.org/10.1021/ac202137y

Lu, X., & Ye, M. (2015). Inertia-Enhanced Pinched Flow Fractionation. *Analytical Chemistry*, *87*(8), 4560–4565. https://doi.org/10.1021/acs.analchem.5b00752

MacDonald, M. E., Spalding, G. C., & Dholakia, K. (2003). Microfluidic sorting in an optical lattice. *Nature*, *426*(6965), 421–424. https://doi.org/10.1038/nature02144

Manz, A., Graber, N., & Widmer, H. R. (1990). Miniaturized total chemical analysis systems: A novel concept for chemical sensing. *Sensors and Actuators B-chemical*, *1*(1–6), 244–248. https://doi.org/10.1016/0925-4005(90)80209-i

Milne, G., Rhodes, D., MacDonald, M. J., & Dholakia, K. (2007). Fractionation of polydisperse colloid with acousto-optically generated potential energy landscapes. *Optics Letters*, *32*(9), 1144. https://doi.org/10.1364/ol.32.001144

Miltenyi, S., Müller, W. E., Weichel, W., & Radbruch, A. (1990). High gradient magnetic cell separation with MACS. *Cytometry*, *11*(2), 231–238. https://doi.org/10.1002/cyto.990110203

Minerick, A. R., Zhou, R., Takhistov, P. V., & Chang, H. (2003). Manipulation and characterization of red blood cells with alternating current fields in microdevices. *Electrophoresis*, *24*(21), 3703–3717. https://doi.org/10.1002/elps.200305644

Mortazavi, S., & Bayareh, M. (2009). *Geometry effects on the interaction of two equal-sized drops in simple shear flow at finite Reynolds numbers*. https://doi.org/10.2495/mpf090321

Murshed, S. M. S. (2021). Introductory Chapter: An Overview of Advances in Microfluidics and Nanofluids Technologies. In *IntechOpen eBooks*. https://doi.org/10.5772/intechopen.98425

Ning, S., Liu, S., Xiao, Y., Zhang, G., Cui, W., & Reed, M. (2021). A microfluidic chip with a serpentine channel enabling high-throughput cell separation using surface acoustic waves. Lab on a Chip, 21(23), 4608–4617. https://doi.org/10.1039/d1lc00840d

Norris, J. V., Evander, M., Horsman-Hall, K. M., Nilsson, J., Laurell, T., & Landers, J. P. (2009). Acoustic Differential Extraction for Forensic Analysis of Sexual Assault Evidence. *Analytical Chemistry*, *81*(15), 6089–6095. https://doi.org/10.1021/ac900439b

Ozcelik, A. (2022). 3D Printed Device for Separation of Cells and Particles by Tilted Bulk Acoustic Wave Actuation. Actuators, 11(9), 249. https://doi.org/10.3390/act11090249

Pamme, N. (2007). Continuous flow separations in microfluidic devices. *Lab on a Chip*, *7*(12), 1644. https://doi.org/10.1039/b712784g

Pandey, S., Mehendale, N., & Paul, D. (2018). Single-Cell Separation. In *Springer eBooks* (pp. 1–28). https://doi.org/10.1007/978-981-10-4857-9_6-1

Park, J. Y., & Jung, H. I. (2009). Multiorifice flow fractionation: continuous size-based separation of microspheres using a series of contraction/expansion microchannels. *Analytical Chemistry*, *81*(20), 8280–8288. https://doi.org/10.1021/ac9005765

Petersson, F., Åberg, L., Swärd-Nilsson, A. A., & Laurell, T. (2007). Free Flow Acoustophoresis: Microfluidic-Based Mode of Particle and Cell Separation. *Analytical Chemistry*, *79*(14), 5117–5123. https://doi.org/10.1021/ac070444e

Pohl, H. A., Pollock, K. G., & Crane, J. S. (1978). Dielectrophoretic force: A comparison of theory and experiment. *Journal of Biological Physics*, *6*(3–4), 133–160. https://doi.org/10.1007/bf02328936

Qin, D., Xia, Y., & Whitesides, G. M. (2010). Soft lithography for micro- and nanoscale patterning. Nature Protocols, 5(3), 491–502. https://doi.org/10.1038/nprot.2009.234

Rivet, C. A., Lee, H. W., Hirsch, A. D., Hamilton, S., & Lu, H. (2011). Microfluidics for medical diagnostics and biosensors. *Chemical Engineering Science*, *66*(7), 1490–1507. https://doi.org/10.1016/j.ces.2010.08.015

S. R. Risbud and G. Drazer, (2014), “Mechanism governing separation in microfluidic pinched flow fractionation devices,” Microfluid. Nanofluidics, vol. 17, no. 6, pp. 1003–1009.

Sajeesh, P., & Sen, A. (2014). Particle separation and sorting in microfluidic devices: a review. *Microfluidics and Nanofluidics*, *17*(1), 1–52. https://doi.org/10.1007/s10404-013-1291-9

Salafi, T., Zeming, K. K., & Zhang, Y. (2017). Advancements in microfluidics for nanoparticle separation. *Lab on a Chip*, *17*(1), 11–33. https://doi.org/10.1039/c6lc01045h

Santana, S. M., Antonyak, M. A., Cerione, R. A., & Kirby, B. (2014). Microfluidic isolation of cancer-cell-derived microvesicles from hetergeneous extracellular shed vesicle populations. *Biomedical Microdevices*, *16*(6), 869–877. https://doi.org/10.1007/s10544-014-9891-z

Schaaf, C. P., & Stark, H. (2017). Inertial migration and axial control of deformable capsules. *Soft Matter*, *13*(19), 3544–3555. https://doi.org/10.1039/c7sm00339k

Segré, G., & Silberberg, A. (1961). Radial Particle Displacements in Poiseuille Flow of Suspensions. *Nature*, *189*(4760), 209–210. https://doi.org/10.1038/189209a0

Shah, S. M. (2018). *Microfluidic Platform to Create Micro Vortices to Enhance the Capture Cancer Stem Cells* (Doctoral dissertation, San Diego State University).

Shao, X., Yu, Z., & Sun, B. (2008). Inertial migration of spherical particles in circular Poiseuille flow at moderately high Reynolds numbers. *Physics of Fluids*, *20*(10), 103307. https://doi.org/10.1063/1.3005427

Shardt, O., Mitra, S. K., & Derksen, J. (2012). Lattice Boltzmann simulations of pinched flow fractionation. *Chemical Engineering Science*, *75*, 106–119. https://doi.org/10.1016/j.ces.2012.03.013

Shi, J., Huang, H., Stratton, Z., Huang, Y., & Huang, T. J. (2009). Continuous particle separation in a microfluidic channel via standing surface acoustic waves (SSAW). *Lab on a Chip*, *9*(23), 3354. https://doi.org/10.1039/b915113c

Shiri, F.; Feng, H.; Gale, B.K. Passive and Active Microfluidic Separation Methods. In Particle Separation Techniques; Elsevier: Amsterdam, The Netherlands, 2022; pp. 449–484

Sivaramakrishnan, M., Kothandan, R., Govindarajan, D. K., Meganathan, Y., & Kandaswamy, K. (2020). Active microfluidic systems for cell sorting and separation. *Current Opinion in Biomedical Engineering*, *13*, 60–68. https://doi.org/10.1016/j.cobme.2019.09.014

Stott, S. L., Hsu, C., Tsukrov, D., Yu, M., Miyamoto, D. T., Waltman, B. A., Rothenberg, S. M., Shah, A. M., Smas, M. E., Korir, G. K., Floyd, F. P., Gilman, A. J., Lord, J. B., Winokur, D., Springer, S., Irimia, D., Nagrath, S., Sequist, L. V., Lee, R. T., . . . Toner, M. (2010). Isolation of circulating tumor cells using a microvortex-generating herringbone-chip. *Proceedings of the National Academy of Sciences of the United States of America*, *107*(43), 18392–18397. https://doi.org/10.1073/pnas.1012539107

Suresh, S. (2007). Biomechanics and biophysics of cancer cells☆. *Acta Biomaterialia*, *3*(4), 413–438. https://doi.org/10.1016/j.actbio.2007.04.002

Tay, F. E. H., Yu, L., Pang, A. J., & Iliescu, C. (2007). Electrical and thermal characterization of a dielectrophoretic chip with 3D electrodes for cells manipulation. *Electrochimica Acta*, *52*(8), 2862–2868. https://doi.org/10.1016/j.electacta.2006.09.022

Unger, M. A., Chou, H., Thorsen, T., Scherer, A., & Quake, S. R. (2000). Monolithic Microfabricated Valves and Pumps by Multilayer Soft Lithography. Science, 288(5463), 113–116. https://doi.org/10.1126/science.288.5463.113

Volpe, A., Gaudiuso, C., & Ancona, A. (2019). Sorting of Particles Using Inertial Focusing and Laminar Vortex Technology: A Review. Micromachines, 10(9), 594. https://doi.org/10.3390/mi10090594

Yamada, M., & Seki, M. (2005). Hydrodynamic filtration for on-chip particle concentration and classification utilizing microfluidics. *Lab on a Chip*, *5*(11), 1233. https://doi.org/10.1039/b509386d

Yamada, M., & Seki, M. (2006). Microfluidic particle sorter employing flow splitting and recombining. Analytical chemistry, 78(4), 1357–1362. https://doi.org/10.1021/ac0520083

Yamada, M., Nakashima, M., & Seki, M. (2004). Pinched Flow Fractionation: Continuous Size Separation of Particles Utilizing a Laminar Flow Profile in a Pinched Microchannel. *Analytical Chemistry*, *76*(18), 5465–5471. https://doi.org/10.1021/ac049863r

Yang, S., Ündar, A., & Zahn, J. D. (2006). A microfluidic device for continuous, real time blood plasma separation. *Lab on a Chip*, *6*(7), 871–880. https://doi.org/10.1039/b516401j

Yin, P., Zhao, L., Chen, Z., Jiao, Z., Shi, H., Hu, B., Yuan, S., & Tian, J. (2020). Simulation and practice of particle inertial focusing in 3D-printed serpentine microfluidic chips via commercial 3D-printers. Soft Matter, 16(12), 3096–3105. https://doi.org/10.1039/d0sm00084a

Zeming, K. K., Thakor, N. V., Zhang, Y., & Chen, C. (2016). Real-time modulated nanoparticle separation with an ultra-large dynamic range. *Lab on a Chip*, *16*(1), 75–85. https://doi.org/10.1039/c5lc01051a

Zhang, J., Li, W., Li, M., Alici, G., & Nguyen, N. (2014). Particle inertial focusing and its mechanism in a serpentine microchannel. *Microfluidics and Nanofluidics*, *17*(2), 305–316. https://doi.org/10.1007/s10404-013-1306-6

Zhao, Q., Yuan, D., Zhang, J., & Li, W. (2020). A Review of Secondary Flow in Inertial Microfluidics. Micromachines, 11(5), 461. https://doi.org/10.3390/mi11050461

Zheng, S., Liu, J., & Tai, Y. (2008). Streamline-Based Microfluidic Devices for Erythrocytes and Leukocytes Separation. *Journal of Microelectromechanical Systems*, *17*(4), 1029–1038. https://doi.org/10.1109/jmems.2008.924274

REPUBLIC OF TÜRKIYE

AYDIN ADNAN MENDERES UNIVERSITY

GRADUATE SCHOOL OF NATURAL AND APPLIED SCIENCES

SCIENTIFIC ETHICAL STATEMENT

I hereby declare that I composed all the information in my master's thesis entitled INVESTIGATION OF THE LOW-COST PASSIVE ON-CHIP CELL SEPARATION METHODS within the framework of ethical behavior and academic rules, and that due references were provided and for all kinds of statements and information that do not belong to me in this study in accordance with the guide for writing the thesis. I declare that I accept all kinds of legal consequences when the opposite of what I have stated is revealed.

Osman GÜLER

… / … / 2023

CURRICULUM VITAE

Last name, First name **:** GULER, Osman

Nationality **:** Turkish

Foreign language **:** English

Education **:** Energy Systems Engineering – Yaşar University

Level	**Institute**	**Date of graduation**
Master's	Natural and Applied Science Institute	
Bachelor's	Faculty of Engineering	30/06/2020

WORK EXPERIENCE:

Year	**Place /Institute**	**Title**
2022	EYS Endüstri Makina San. ve Tic. A.Ş.	Project Engineer